

**Arc Foundations and the initiation of subduction
in the Izu-Bonin Forearc**

A Thesis Presented to
the Faculty of the Department of Earth and
Atmospheric Sciences
University of Houston

In Partial Fulfillment
of the Requirements for the Degree
Master of Science

By
Matthew Loocke

May 2013

ARC FOUNDATIONS AND THE INITIATION OF SUBDUCTION IN THE IZU-BONIN FOREARC

Matthew Phillip Loocke

APPROVED:

Dr. Jonathan E. Snow, Department of
Earth and Atmospheric Sciences

Dr. Alan Brandon, Department of Earth
and Atmospheric Sciences

Dr. Henry J.B. Dick, Department of
Geology and Geophysics, Woods Hole
Oceanographic Institute

NSM Dean, College of Natural Sciences
and Mathematics

ACKNOWLEDGEMENTS

I would like to first and foremost thank my family for supporting me through my entire undergraduate and graduate careers. Their constant encouragement for me to follow my passions and become a research scientist has been a source of enormous pride and confidence when I have needed it most. The most important cultivator of my present and future career has been my advisor and close friend, Jon Snow. Since my beginnings as a business major in his excellent Honors Introduction to Geology course, he has managed to encourage me to do such ‘asinine’ things as switch my major, conduct research, and accompany him on several academic research cruises. Jon allowed me, a low GPA, passionate undergraduate, to have free-reign of the laboratory to develop and conduct research on my own with only the lightest of guiding hands. Without Jon, I would not be the driven, independent researcher that I am today. With Jon, I carried out what became my Senior Honors Thesis (Temporal variations of melt stagnation in a back-arc lithospheric section: Systematics of plagioclase impregnation in mantle rocks from the Godzilla Megamullion) and this completed Graduate Thesis along with several other ongoing projects. Jon is to blame for me being introduced to my good friend, mentor, and possible aged doppleganger, Henry Dick. Henry has served as a source of inspiration and enormous support over the course of the past few years. Through many fruitful scientific discussions and many more tippie soaked conversations regarding what not to do with your career, Henry has strongly influenced my life and my career.

Many other geologists have contributed a great deal of nurturing and influence over the past few years including Tom Lapen, Jack Casey, and my good friends Alan Brandon and Esteban Gazel. Esteban has been a great friend, occasional teacher, and

close collaborator who I look forward to continue working with. Alan has provided me with a wealth of knowledge regarding isotope geochemistry and facilities to freely conduct Re-Os chemistry in. Most of all he has been a source of constant encouragement and an ear to vent to when needed. Speaking of ears and venting, Wendy Nelson deserves a medal or possibly a nice dinner for everything she has had to put up with. Wendy served as a surrogate advisor while Jon was at sea and has provided both encouragement and cautionary advice during my weekly venting sessions. Thanks for always having your door open and being there when I needed it. Without my fellow students and doughboys in the trenches, Shawn Wright, Jesse Dietderich, Thera Grosshans, Alex Barnard, Barry Shaulis, and Curtis Calva, I could not have made it all these years. Your constant venting reminded me I wasn't going through this alone. You guys were always there when I needed help. You were always there to let me know when I was thinking too much and needed to take a break. You even knew when liquid encouragement was needed by uttering phrases like "Let's just go the saucer" or "Beer?" Speaking of which, I need to thank the Flying Saucer Draught Emporium and the various Houston area micro-breweries. It may be considered 'inappropriate' to address this in this setting, but I am a geologist. They have provided me with a means to clear my head and take a break along with my friends and family when things got tough or breaks needed to be had.

To all of you: Thanks for the past few years. Here's to a promising career and bright future! Cheers, Prosit, Kampai, Salut, Pura Vida, Sante, Slainte, and Eis Igian!

**ARC FOUNDATIONS AND THE INITIATION OF
SUBDUCTION IN THE IZU-BONIN FOREARC**

An Abstract of a Thesis

Presented to

the Faculty of the Department of Earth and

Atmospheric Sciences

University of Houston

In Partial Fulfillment

of the Requirements for the Degree

Master of Science

By

Matthew Loocke

May 2013

ABSTRACT

Our understanding of the lower crust in the ocean basins has been inferred from geophysical studies of mid-ocean ridges (MOR), volcanic arcs, and ophiolites. Many studies of ophiolites suggest that although they exhibit characteristics of MOR's, they may originate in supra-subduction zone (SSZ) settings. It is also suggested that the foundations and lower crust of SSZ arcs are created by a MOR, possibly in a trench-ridge-trench triple junction setting. Although many samples of the lower crust have been collected along the world's MOR's, few samples have been retrieved from SSZ arcs.

Fifty ultramafic and gabbroic samples recovered by dredges 31 and 42 of the KH07-02 dredging cruise along the inner trench wall of the Izu-Bonin Arc have been characterized as lower crustal rocks related to MOR-like basalts (fore-arc basalts or FAB). Major element analyses of Cr-spinels indicate two distinct compositional trends. Group M consists of wehrlites and gabbros with medium Cr# (45-60) and high Al_2O_3 and TiO_2 (12-30 & 0.1-2.25 wt. %) which reacted with MORB-like melts. Group B consists of spinels solely from dunites and peridotites with high Cr# (65-94) and low Al_2O_3 and TiO_2 (3-21 & 0-0.12 wt. %) which reacted with boninitic melts. Boninites from the Bonin Ridge are known to be younger (44-48 Ma) than FABs (50-52 Ma). This suggests that the majority of the lower crust was related to subduction initiation.

Major and trace element analyses of clinopyroxenes associated with Group M spinels indicates highly depleted compositions characteristic of high degree partial melts or boninites. A lack of orthopyroxene and association with Group M spinel suggests that D31 clinopyroxenes evidence singly depleted, un-aggregated melt fractions. This

suggests that FABs are the result of mixing between a highly depleted mantle source and a MORB-like liquid. Modeling results in 5 to 7% fractional melts of DMM refertilized by the addition of ~12% N-MORB reproducing such a mixing array. This model is consistent with models for subduction initiation which suggest that asthenosphere will upwell into the void created between the down-going and overriding plates during initiation and begin to undergo decompression melting.

TABLE OF CONTENTS

ABSTRACT	v
INTRODUCTION	1
The Philippine Sea Plate: A Complex Tectonic History	3
The IBM Forearc and Ophiolites	6
Subduction Initiation and the IBM Arc System.....	9
Lower Crustal Sampling of the Bonin Ridge	11
ANALYTICAL METHODS.....	16
Major Element Analysis.....	16
Trace Element Analysis	17
RESULTS.....	18
Petrography	18
Mineral Chemistry	22
Spinel	22
Olivine	26
Pyroxene.....	28
Trace Element Geochemistry	33
DISCUSSION	36
Melt Stagnation and Melt-rock Reaction in the Lower Crust	36
Contrasting MORB-Boninite Reaction Trends in the Bonin Ridge Lower Crustal Spinels	42
Ultra-depleted Melts and the Formation of FAB.....	44
CONCLUSIONS.....	51
REFERENCES	54
APPENDIX 1: ANALYTICAL METHODS AND PROCEDURES	71
Electron Microprobe Methods	71
Laser Ablation-Inductively Coupled Mass Spectrometry (LA-ICP-MS)	75
APPENDIX 2: PETROGRAPHIC OBSERVATIONS.....	77

LIST OF FIGURES

Figure 1: Philippine Sea and Bonin Ridge Bathymetric Maps	2
Figure 2: Bonin Ridge Stratigraphy.....	5
Figure 3: Bathymetric Track for Dredge D31 and Dive 7K417	13
Figure 4: Representative Photomicrographs.....	20
Figure 5: Spinel Cr# vs Mg# and TiO_2 and Al_2O_3 vs TiO_2	25
Figure 6: Olivine Mg# vs NiO	28
Figure 7: Clinopyroxene Mg# vs TiO_2 , Na_2O , and Al_2O_3	31
Figure 8: Clinopyroxene Cr_2O_3 vs TiO_2	32
Figure 9: CI-Chondrite Normalized Clinopyroxene REE Spider Plots	35
Figure 10: Estimated D31 Pyroxene-Plagioclase-Olivine Modal Abundances.....	41
Figure 11: Zr vs Ti of FABs and Modeled Melts	48
Figure 12: Schematic Model for Melting During Subduction Initiation	50
Figure A2.1: IUGS Ultramafic-Mafic Plutonic Igneous Rock Ternary	77

LIST OF TABLES

Table 1: Important Sampling Sites.....	8
Table 2: Spinel Major Element Analyses	23
Table 3: Olivine Major Element Analyses	27
Table 4: Pyroxene Major Element Analyses	30
Table 5: LA-ICP-MS Analyses of Clinopyroxene.....	34
Table A1.1: EMP Standard Compositions.....	71
Table A1.2: EMP Spinel Analytical Conditions for UH.....	72
Table A1.3: EMP Olivine Analytical Conditions for TAMU	72
Table A1.4: EMP Clinopyroxene Analytical Conditions for TAMU	72
Table A1.5: EMP Orthopyroxene Analytical Conditions for TAMU	73
Table A1.6: EMP Spinel Analytical Conditions for TAMU	73
Table A2.1: Petrographic Thin Section Descriptions	78

INTRODUCTION

Oceanic subduction is one of the key processes in plate tectonics (Ampferer, 1906; Amstutz, 1951; White et al., 1970). Although the volcanic portions of subduction zones are well studied, comparatively little is known about the formation of the lower arc crust. Most of current thinking in this regard has been extrapolated from studies of ophiolites (e.g. Oman, Troodos, and the Alpine Ophiolites) (see Pearce, 2003 for a historical perspective) due to the rarity of in-situ lower arc crust. For decades, the Izu-Bonin-Mariana (IBM) forearc has been considered a type locality for processes governing subduction initiation and the evolution of volcanic arcs (Meijer, 1980; Fryer et al., 1992; Stern and Bloomer, 1992; Bloomer et al., 1995; Kodaira et al., 2010; Ishizuka et al., 2011). The subaerial forearc exposures on the Ogasawara Islands (Reagan and Meijer, 1984; Umino, 1985) and the recovery of early-arc lavas from deep dredging along the outer-arc high of the Bonin Ridge (Bloomer, 1983) have provided a basis for the current models of early-arc development and evolution (Pearce et al., 1992; Kodairi et al., 2010; Ishizuka et al., 2011).

The IBM arc system covers a major portion (~5000 km) of the eastern boundary of the Philippine Sea Plate, south of Japan (Fig. 1), which in itself preserves a complex record of the recent geologic history for the western Pacific in its many remnant arcs and marginal basins (Sdrolias et al., 2004 and references therein). Of the many expeditions that have sampled the IBM arc, few have recovered intact mafic and ultramafic plutonic rocks from the lower crust, and even fewer of those samples have been the subject of detailed investigation (Fryer et al., 1992; Ishii et al., 1992; Pearce et al., 1992).

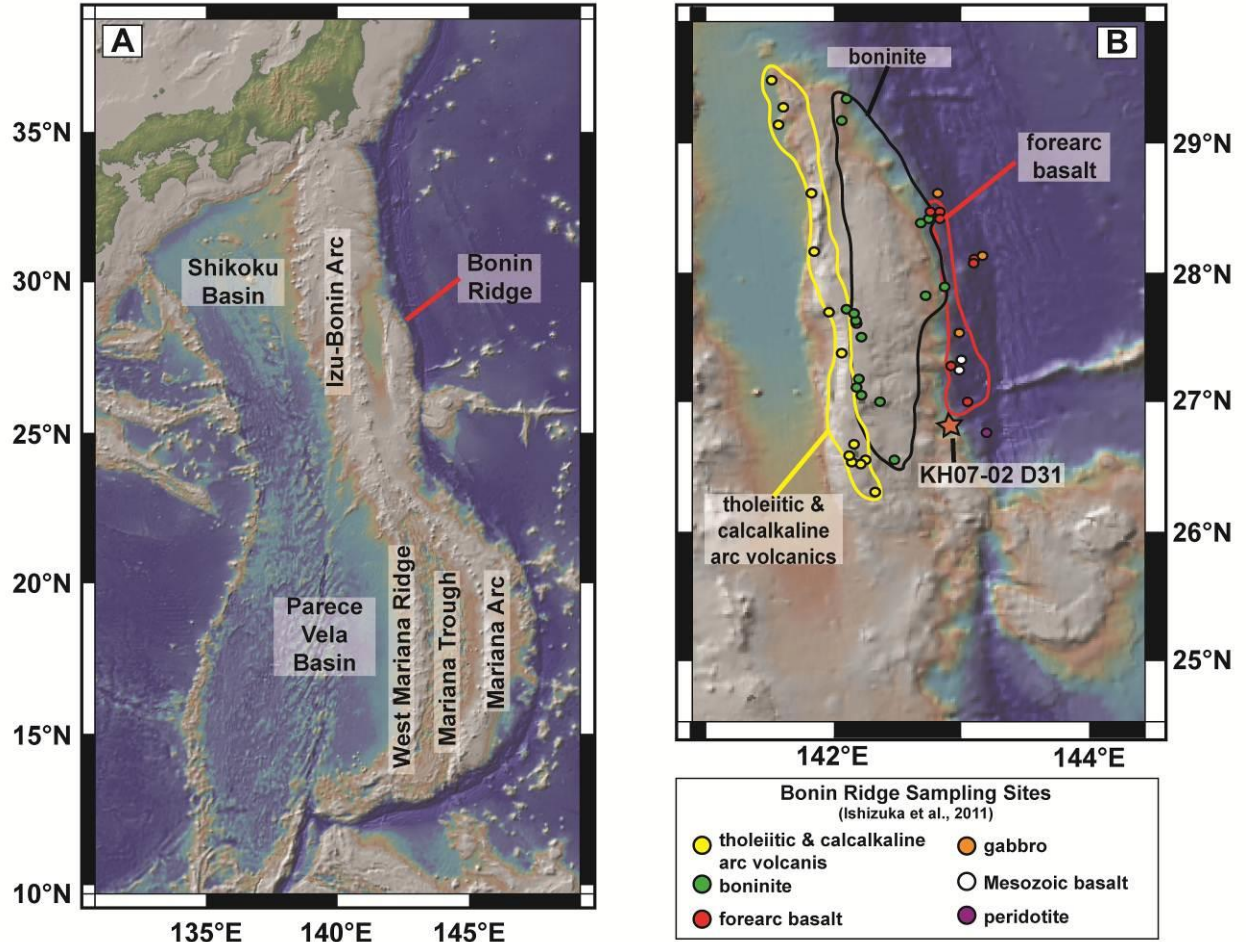


Figure 1: Bathymetric map of the (A) Philippine Sea Plate and the (B) Bonin Ridge.

Sampling sites and lithologies for the Bonin Ridge after Ishizuka et al. (2011). Dredge

D42 is located where the forearc basalt label points. Bathymetry from GeoMap App.

The Philippine Sea Plate: A Complex Tectonic History

The Philippine Sea Plate is located south of Japan and east of the Philippines in the Philippine Sea (Karig et al., 1978; Sdrolias et al., 2004). As a whole, the plate is thought to be the result of a complex history of several arc-lengthening events (i.e. a trench-ridge-trench configuration similar to the West Philippine Basin) and episodic backarc spreading events (Karig et al., 1978; Sdrolias et al., 2004). A general consensus on the major events which led to the current configuration of the eastern margin of the Philippine Sea Plate and its morphology has been made even though many of the details of the events are still under debate (e.g. Karig et al., 1978; Kobayashi and Nakada, 1979; Hussong and Uyeda, 1981; Pearce et al., 1992; Sdrolias et al., 2004). It is estimated that the early arc terrain developed primarily around the inception of subduction in the Eocene (between ~48 to 43 Ma) on through the early Oligocene (between ~34 to 31 Ma; Sdrolias et al., 2004 and references therein). Following this period of early arc development, an episode of back-arc spreading began in the Parece Vela Basin (PVB) which separated the Kyushu-Palau Ridge from the early arc terrain by way of both northward and southward propagating rift tips (between ~31 to 29 Ma). The northern Shikoku Basin later began spreading concurrently with the PVB around 25 Ma with a southward propagating rift that linked the two basins by 23 Ma. After joining, the two basins shared their spreading axis until spreading ceased in the Shikoku Basin at 17-15 Ma and in the PVB between 15-12 Ma. At this point, the active zone of extension moved towards the arc and began to slowly open the currently active Marianas Trough around 8 to 6 Ma which then isolated the West Marianas Ridge remnant arc. Currently the

Marianas Trough is estimated to be propagating northward where it is slowly beginning to rift the Izu-Bonin portion of the IBM arc (Pearce et al., 1992) (Fig. 1).

The lack of a recent, major backarc spreading episode in the Izu-Bonin arc (aside from the estimated Oligocene formation of the Ogasawara Trough) has made it an ideal location for the possible recovery of materials associated with the various early stages of arc and fore-arc development. In particular, submersible dive studies, combined with drilling and dredging of the outer-arc high of the prominent Bonin Ridge (Fig. 1) have returned an overall older (~50 to 30 Ma) lithologic stratigraphy, which closely resembles that of deemed “supra-subduction zone (SSZ)” ophiolites (Ishizuka et al., 2011, and references therein; Figure 2). In an effort to understand the temporal and spatial variations in IBM arc magmatism, several recent studies have cataloged the various volcanic samples recovered and analyzed from the arc and split them into groups based on their age and composition (Reagan et al., 2010; Ishizuka et al., 2011). Two of the most abundant volcanic rocks in the IBM forearc have boninitic and mid-ocean ridge basalt (MORB)-like composition. These MORB-like tholeiitic basalts were given the name forearc basalt (FAB) by Reagan et al. (2010) and interpreted to be related to the first erupting lavas following the initiation of subduction. Dredge and submersible sampling of the deep landward slope of the Bonin Ridge (i.e. Ogasawara Ridge) has recovered lower crustal/upper mantle peridotites and gabbroic rocks in close spatial relationship to FABs. Ishizuka et al. (2011) report U-Pb ages of zircons in 2 isotropic gabbros recovered from separate locations on the ridge with $^{206}\text{Pb}/^{238}\text{U}$ ages of 51.72 ± 0.82 and 51.63 ± 0.79 Ma, which are nearly identical to the oldest $^{40}\text{Ar}/^{39}\text{Ar}$ age for FABs within 2σ error.

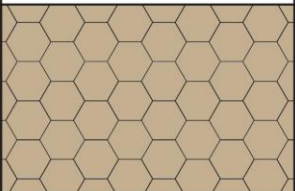

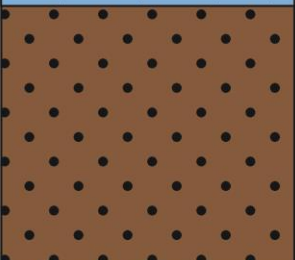


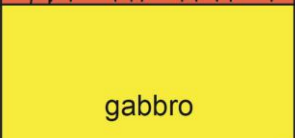


Lithology	Age (Ma)	Approximate Depth	
arc tholeiites and calc-alkaline rocks	37-44	subaerially exposed 5500-4760 6300 6780	
high-Mg andesites	44-45		
boninite, andesite (and their differentiates)	44-48		
basalt (FAB)	50-52		 
gabbro/Mesozoic basalt	50-52		 
peridotite			

Figure 2: Representative stratigraphy for the Bonin Ridge based on dive and dredge sampling after Ishizuka et al. (2011). Beneath 5500 to 4760 m, a sequence of pillow lavas over sheeted dykes followed by gabbros and peridotites has been recovered. This sequence represents a Penrose ophiolite stratigraphy where pillow lavas overly sheeted dykes which root into isotropic gabbros. These isotropic gabbros grade into layered gabbros which overly mantle peridotite at their base (Dick et al., 2006).

The IBM Forearc and Ophiolites

Several investigations have identified the forearc crustal stratigraphy of the IBM arc, inferred from combined sampling of FABs and boninites and various exposures of gabbros and peridotites along the inner trench wall, as being very similar to that of well-preserved ophiolites (Stern, 2004). Peridotite and gabbro assemblages in ophiolites are considered to represent ancient pieces of oceanic lithosphere that have been tectonically emplaced on or against island arcs and continental lithosphere (e.g. Moores and Vine, 1971; Shervais, 2001). The assemblages in ophiolites can range from variably depleted oceanic upper mantle to complex mocho transition zones made up of various gabbroic and ultramafic lithologies. Many investigations of ophiolite complexes have made attempts to tie individual ophiolites to various tectonic settings (e.g. Mid-Ocean Ridges, Supra-subduction Zones, or Backarc Spreading Ridges) with little consensus (e.g. Cann, 1970; Pearce and Cann, 1973; Dick and Bullen, 1984; Pearce, 2003; Morishita et al., 2011b). Although ophiolites can vary largely in their overall structure and stratigraphy, the Penrose model, which was derived from geophysical studies of ophiolites and MOR's, has often been used to represent an ideal ophiolitic stratigraphy that could be created during normal MOR spreading.

Ishizuka et al. (2011) compiled both the age and major and trace element data for samples collected from the Bonin Ridge over the course of multiple diving and dredging expeditions. From the data collected, it was deduced that the volcanic edifice of the Bonin Ridge preserved rocks mostly related to the early stages of arc development with minor amounts of younger arc material. Further, the chemical and structural characteristics of the analyzed FABs were determined to represent material that was

formed in a MOR-type setting unrelated to material being subducted in the western Pacific or early Philippine Basin volcanics. Table 1 provides a synthesis of the rock types, ages, and relative distribution of the samples and important sites used in this study.

Table 1: Summary of diving and dredge sampling results.

Station No.							samples recovered
	Lat (°N)	Lon (°E)	Depth (m)	Lat (°N)	Lon (°E)	Depth (m)	
<i>Shinkai6500 dives</i>							
6K1149	28.469	142.849	6449	28.47	142.831	6024	isotropic gabbro, diabase, basalt (FAB) lava, basaltic
6K1153	28.465	142.833	6112	28.451	142.822	5715	isotropic gabbro, diabase, basalt (FAB) lava, basaltic
6K1154	28.447	142.822	5720	28.457	142.796	5189	isotropic gabbro, diabase, basalt (FAB) lava, basaltic breccia, boninite lava block, sandstone
<i>Kaiko dives</i>							
7K417	26.772	143.206	5792	26.772	143.206	5336	peridotite, gabros, dolerites
7K418	27.289	142.953	5199	27.301	142.94	4303	gabbro, conglomerate
7K419	28.12	143.13	6994	28.119	143.113	6486	peridotite, gabbro, mudstone
7K450-2	28.603	142.838	6941	28.596	142.827	6552	gabbro, basalt (FAB) lava, mudstone
7K452	27.55	143.002	6958	27.555	142.988	6379	gabbro,pyroxenite, basalt (FAB) lava, sandstone
<i>dredge sampling</i>							
KH07-02 D31	26.772	143.206	5738	26.772	143.206	5293	peridotite, troctolite, pyroxnite, gabbro, diorite
KH07-02 D37	27.297	142.946	5069	27.297	142.946	4477	gabbro
KH07-02 D42	28.439	142.848	6336	28.439	142.848	5943	isotropic gabbro, diabase, basalt (FAB) lava, basaltic

Ishizuka et al. (2011) and Reagan et al. (2010) suggest that the FABs are a volcanic product related to processes similar to MOR spreading which occurred during or shortly after subduction initiation, based on the ages and the MORB-like affinity of the FABs. It is generally agreed that subduction initiated along the proto-IBM arc around 50-55 Ma along with several other Western Pacific arcs (e.g. the Tonga-Kermadec) (Stern, 2004). Although there is some consensus, the mechanisms and models for how subduction initiated along the IBM arc are still considered to be under debate.

Subduction Initiation and the IBM Arc System

Two models have been put forward to describe the events that lead to the initiation of subduction. These are the spontaneous nucleation of subduction zone (SNSZ) and the induced nucleation of a subduction zone (INSZ) models (Stern, 2004). The main difference between these two models is that INSZ initiation begins with a period of convergence followed by subsidence, whereas the SNSZ initiation begins with gravitational instability and lithospheric subsidence in the down-going lithospheric plate (Stern (2004) provides great detail on these two models for subduction initiation). In this sense, early reverse faulting, folding, and uplift of the upper plate is expected to result from the compressive regime of thrusting of one plate over the other in the INSZ model. Consequently, a preserved record of extension, normal faulting, seafloor spreading, and/or subsidence in the upper plate would implicate a SNSZ mode of initiation, reflecting the subsidence of the down-going lithospheric plate due to gravitational instability (Stern, 2004). By examining the early sequence of events preserved in the overriding plate, we can distinguish between the spontaneous nucleation of a subduction zone (SNSZ) and the induced nucleation of a subduction zone (INSZ) modes of initiation for a given modern or

ancient (i.e. SSZ ophiolite) subduction zone based on the predicted consequences of the two models.

The IBM arc system has played a huge role in understanding how subduction zones and ophiolites form (Pearce et al. 1992; Pearce, 2003; Stern, 2004; Morishita et al., 2011b). This is in part due to the early record of the subduction system that is preserved in the IBM forearc crust, which is well exposed with limited sediment cover and no accretionary prism (Stern and Smoot, 1998; Stern, 2004). As previously discussed, the forearc crust has been studied in great detail from subaerial island exposures and by drilling, diving, and dredging along the inner trench wall. Although small slivers of ‘trapped’ older crust have been identified (DeBari et al., 1999), it is generally agreed that the exposures of pillow basalts and sheeted dikes and boninites combined with the various gabbro-peridotite exposures sampled along the inner IBM trench wall represent the general lithospheric structure for the entire length of the IBM forearc (Stern et al., 2003). Based on these observations and numerical models which show a sequence of events resulting in the overriding plate undergoing spreading as subduction initiates (Hall et al., 2003; Gurnis et al., 2004), it is agreed that the IBM forearc originated in a SSZ spreading environment at or shortly after the time that subduction began at the trench (Stern et al., 2003). Although much of this evidence points towards a SNSZ model for subduction initiation along the IBM trench, conclusions gleaned from the results of geodynamic modeling suggest an induced model for IBM subduction initiation (Hall et al., 2003; Gurnis et al., 2004). The main objection to the SNSZ model by the geodynamic community is based on their consensus that the oceanic lithosphere is too strong to flex as is needed by the ‘retreating hinge line’ required in the SNSZ model (Stern, 2004). However, serpentinization of the oceanic lithosphere due to re-activation of deep faults by down flexing may weaken the lithosphere enough to accommodate the amount of

lithospheric flexure needed for the ‘retreating hinge line’ (Ranero et al., 2003; Ranero et al., 2004).

Despite these objections, an overwhelming amount of evidence supports a SNSZ origin for the IBM arc system. Aside from the abundance of igneous activity over a broad region of the IBM forearc, it is noted that there are data to suggest that the Tonga-Kermadec convergent margin began roughly about the same time as the IBM arc system at about 45-50 Ma (Bloomer et al., 1995; Stern, 2004). The SNSZ model implies that subduction will initiate nearly simultaneously along the ‘downstream’ margins of the affected plate. Thus, there is a general consensus that the IBM arc system roughly conforms to a SNSZ model for subduction initiation. This consensus is dominantly based on focused studies on the Marianas forearc and the Bonin Ridge. As previously mentioned, the earliest volcanics and plutonics of the Bonin Ridge (i.e. the FABs and gabbros) have a tight age range of 50-52 Ma and are suggested to be associated with MOR-like magmatism in response to subduction initiation. However, dating of gabbroic zircons by Ishizuka et al. (2011) has been the only work that has been carried out on the lower crustal gabbros and peridotites recovered from the Bonin Ridge, aside from a small study of a handful of peridotites from the 7K417 dive site (Morishita et al., 2011b).

Lower Crustal Sampling of the Bonin Ridge

Of the 19 stations dredged along the Bonin Ridge, many of the dredges below 6000 m recovered some amount of gabbroic and/or ultramafic rock with a few dredges above 6000 m returning gabbroic rock (Ishizuka et al., 2011). The sampling of ultramafic rocks by these dredges marked the first recovery of ultramafic rocks along the Izu-Bonin arc outside of the previously sampled serpentine seamounts (e.g. Ishii et al., 1992; Pearce et al., 1992).

During the R/V Hakuho Maru KH07-02 cruise, dredge stations located on the deep

landward slope of the Bonin Ridge recovered FAB pillow basalts as well as gabbroic and ultramafic rocks. This is noted as the first recovery of peridotite from the Izu-Bonin arc, aside from the ODP leg 125 sampling of the serpentine seamounts (Tani et al., 2009; Ishizuka et al., 2011). Dredge 31 (D31) was located on the trench wall of the Bonin Ridge, east off of the Hahajima Islands. D31 dredged from 26°46.15'N, 143°12.85'E at 5738 m to 26°46.34'N, 143°12.34'E at 5293 m and recovered peridotite, wehrlite, pyroxenite, gabbro, and diorite (see Figure 1 and 3). This same sampling path was followed by the ROV Kaiko Dive 7K417, which sampled the same lithologies (Fig. 3). Submersible and ROV investigations along the trench slope of the Bonin Ridge, such as Kaiko Dive 7K417, have recovered similar lithologies from outcrops. Spatial relationships observed by the dives were used to determine that the outcrops are slopes of a tectonically exposed lower-crustal/mantle derived peridotite and gabbro body. This body was probably developed by the IBM arc instead of a less likely origin from the serpentine seamounts which are interpreted to be the result of serpentine diapirs (Morishita et al., 2011b).

□□

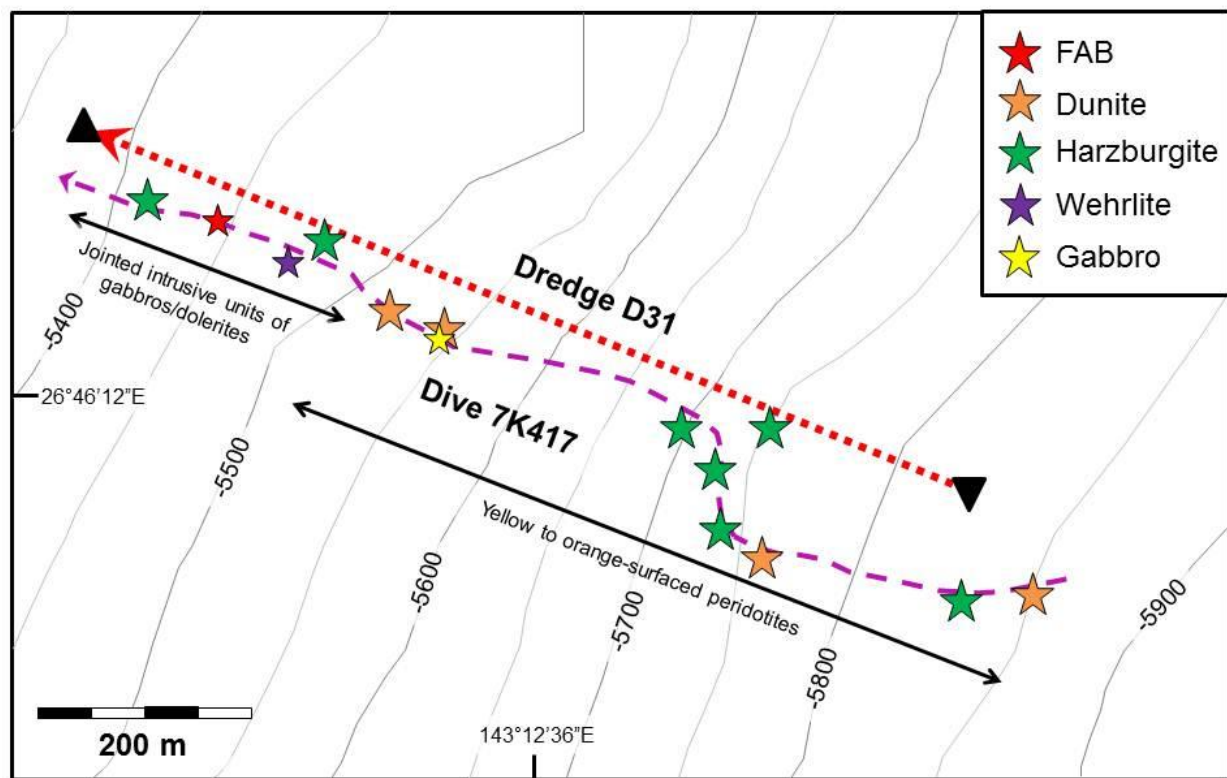


Figure 3: A bathymetric map showing the tracks of dredge D31 and Dive 7K417 (red dashed and purple dashed lines respectively), and the sampling points for Dive 7K417. The colored symbols show the dominant lithologies collected at each sampling point. A diabasic sample with FAB chemistry is represented by the red star. (after Morishita et al., 2011b; Harigane et al., in prep).

The samples chosen for this study consist of residual peridotites (i.e. dunites and harzburgites), wehrlites, and gabbros recovered from dredges D31 and D42 of the R/V Hakuho Maru KH07-02 Leg 2 dredging cruise. Dredge D42 also recovered fragments of variably altered pillow basalts and hyaloclastite (composed of relatively fresh basaltic and glass fragments) that were interpreted to have originated similarly to basalts from fore-arc highs or oceanic basement where the Izu-Bonin arc was built. The extant thin section collection for dredges D31 and D42 includes a total of 50 thin sections (D31: 35 sections; D42: 15 sections).

The composition of lower-arc crust is poorly understood. These samples provide a source of in-situ lower arc crust that can be examined in detail. Although SSZ arcs are typically treated as distinctly separate environments from MOR's, questions regarding how similar, or different, SSZ arc lower crust to that of MOR's and BAB's can be addressed by the study of these rocks. In particular, are the processes of lower crustal melt migration similar to those seen at slow spreading ridges (Godard et al., 2008; Suhr, 2004) and back-arc basins (Sanfilippo et al., 2013)? It is suggested that due to the drastically different tectonic settings, the processes of crustal accretion and melt migration will possibly behave in slightly different ways. However, the relationships between the samples examined in this study and those recovered from other tectonic settings may indicate that the difference in tectonic setting does not make a difference regarding the processes of melt migration and crustal accretion in the lower crust.

Previous studies of primitive gabbros, peridotites, and associated lavas in ophiolites have been successful in recognizing geochemical relationships which tie phases within the hybridized plutonic rocks of the lower crust to known melt compositions through geochemical modeling (e.g. Kelemen et al., 1997; Python and Ceuleneer, 2003; Tribuzio et al., 2008). Many ophiolites, such as Oman, have been interpreted to originate in a SSZ setting, but also exhibit evidence for MOR-type melt compositions (Dick and Bullen, 1984; Kelemen et al., 1997; Pearce, 2003). Although the samples under study are spatially/temporally associated with the FABs, there is a possibility that they share a common origin with later migrating boninitic melts. Ideally, the trace element chemistry of the samples could be used to determine if they are consistent with an origin relating to the FABs or the later boninites.

We present a detailed examination of the petrographic and geochemical nature of 50 ultramafic and gabbroic lower arc samples recovered from dredges D31 and D42 of the R/V

Hakuho Maru KH07-02 dredging cruise along the Izu-Bonin inner trench wall. The relict phases in the ultramafic and gabbroic samples of D31 and D42 provide geochemical data that can constrain mantle processes such as the mechanisms of melt extraction, the degree of partial melting, and melt-rock interaction (e.g. Kelemen et al., 1992; Johnson et al., 1990; Hellebrand et al., 2001). Further, the rarity of the samples under study makes the data derived from them important to our understanding of the nature and composition of the lower arc crust, the foundations that suprasubduction zone arcs are built on, and the processes governing magmatism during subduction initiation.

ANALYTICAL METHODS

The 50 thin sections were described, including detailed microscopic observations and high resolution scans of the thin sections in both plain polarized light and cross-polarized light. They were then carbon coated and prepared for geochemical analysis.

Major Element Analysis

Major element analyses were carried out using the electron microprobe (EMP) facilities at The University of Houston, and Texas A&M University. Spinels were measured using the Cameca SX-50 EMPs at the University of Houston and Texas A&M. Analyses used an accelerating potential of 15kV, a beam current of 20nA, and spot sizes of 1 micron. Counting times were 20 s for Zn, Mn, Mg, Si, Al, and Cr, 60 s for Ti and Ni, and 40 s for Fe. Orthopyroxene, clinopyroxene, and olivine major element data were collected using the Cameca SX-50 facilities at Texas A&M University with only orthopyroxene and clinopyroxene being analyzed at the University of Houston using an accelerating potential of 15kV, a beam current of 20nA, and beam sizes of 1 micron. Counting times for orthopyroxene and clinopyroxene were 20 s for Na, 60 s for Mg, 45 s for Si and Al, and 30 s for K, Ca, Ti, Cr, Mn and Fe. Counting times for olivine were 20s for Fe, 40 s for Mg and Si, 60 s for Ni and Mn, 70 s for Ca and Ti, and 100 s for Al. To verify that the analytical results had not been varied significantly by mechanical drift, sample analyses were interspersed with standard analyses. Analyses were rejected if their totals were greater than 101% or less than 98% and if they showed evidence for mixed analysis or phase misidentification (e.g. SiO₂ in spinel).

Trace Element Analysis

Trace elements were measured in-situ for clinopyroxenes using a Varian quadrupole inductively coupled plasma mass spectrometer (ICP-MS) with a CETAC Nd-YAG laser ablation sampled introduction system (213 nm laser wavelength) at the University of Houston. Grains previously measured by electron microprobe in thin sections were measured in-situ with the laser at a 5 Hz shot rate ranging from 150 to 170 bursts (i.e. 30 to 40 second measurement times). Only 1 to 2 grains in each sample were suitable for laser ablation with an average of 3 to 5 spots per grain. Spot sizes of 100 μm were used. Data reduction was performed by a Linux-based in-house developed laser ablation reduction software package. Laser beam penetration through the clinopyroxene was monitored during analysis and removed automatically by the data reduction software. Calcium concentrations determined by electron microprobe analysis were used to correct the measured trace element ratio concentrations for drift over the course of an analytical run. A more detailed analytical procedure for the microprobe as well as the LA-ICP-MS can be found in Appendix 1.

RESULTS

Petrography

Due to modal variations (e.g. on the order of 10%) of olivine, clinopyroxene, orthopyroxene, and plagioclase, which we infer might reflect gradual transitions between lithologies, within the samples under study, a slightly altered version of the IUGS classification was used to simplify the samples for comparison. However, each sample is identified according to the IUGS classification of Streckeisen (1967) in the table of petrographic observations located in appendix 2 (i.e. table A2.1). Peridotites that are heavily altered and cannot be categorized along with those identified as harzburgites are referred to as harzburgites. Samples containing modal plagioclase $\leq 5\%$ and clinopyroxene $\geq 5\%$, which include wehrlites, plagioclase-wehrlites, and pyroxenites, are referred to as wehrlites. The D31 samples consist of 22 peridotites, 7 plagioclase-bearing peridotites and wehrlites, 2 pyroxenites, 1 gabbro, and 3 orthopyroxene-bearing olivine-gabbros. The 7 plagioclase-bearing peridotite and wehrlites were originally identified as troctolites by the shipboard scientific crew, but closer investigation revealed that they are in fact wehrlites/peridotites and plagioclase-wehrlites/peridotites. The D42 samples consist of 14 oxide-bearing gabbros (oxides ~ 1 to 7 vol. %) and 1 dunite. The D42 oxide-gabbros are directly related to gabbros analyzed by Ishizuka et al. (2011), which are under further investigation, and thus were only examined petrographically for this study.

Alteration is variable in the D31 peridotites, pyroxenites, and wehrlites, ranging from heavy red-orange oxidation or total serpentinization in most to nearly fresh samples (Fig. 4). Alteration has left a majority of the samples with very few, tiny primary relict silicate phases (Fig. 4). Spinel is a common phase in various sizes and shapes, which is generally found

conforming to a foliation in the silicates where preserved. Although alteration of the peridotite samples in many cases is extensive, a small number of samples were determined to be dunites, and 2 samples were clinopyroxene-bearing harzburgites (Fig. 4). The plagioclase-bearing peridotites, wehrlites, and gabbros also suffer from heavy alteration, with pyroxenes and plagioclase having been altered to amphibole and prehnite \pm chlorite \pm hydrogrossular respectively. The plagioclase-bearing peridotites and wehrlites exhibit textures that may indicate they were produced by melt infiltration along grain boundaries (Fig. 4).

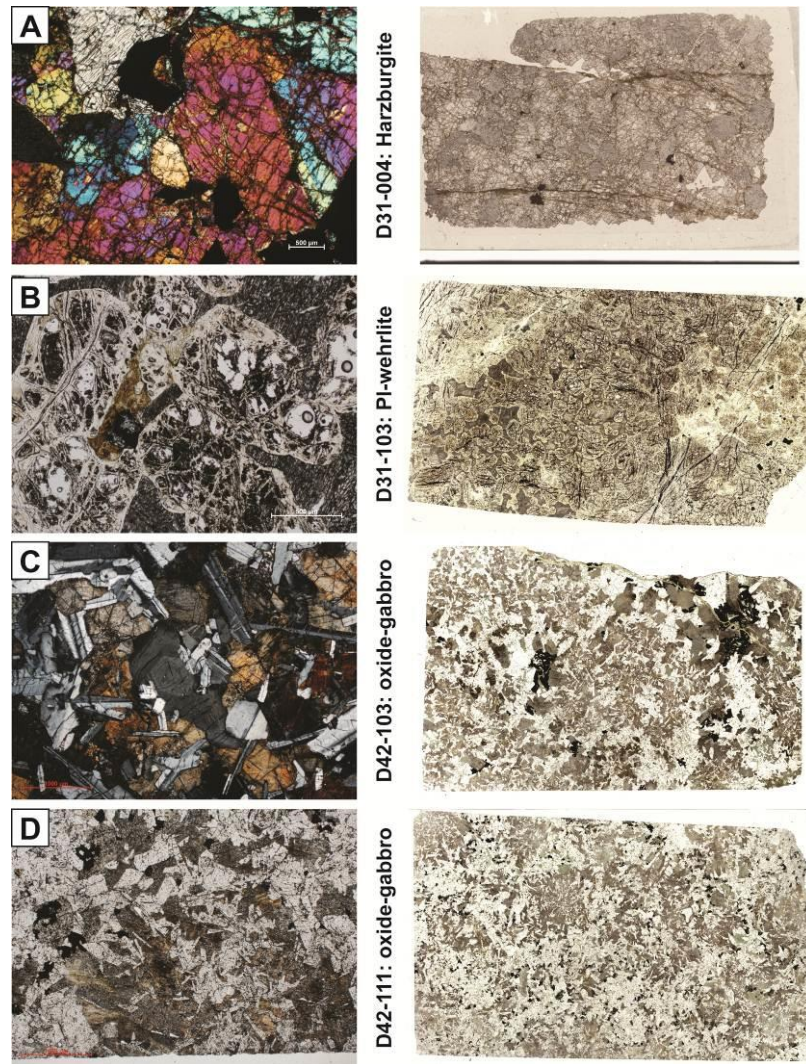


Figure 4: Representative photomicrographs of samples from dredges D31 and D42. Each photo is accompanied by a full thin section scan to the right. (A) KH07-02 D31-004 (cross polarized light): a granular harzburgite with olivine, orthopyroxene, and large holly leaf spinels; (B) KH07-02 D31-103 (plain polarized light): a plagioclase-wehrlite with cumulate olivine surrounded by large clinopyroxene crystals; (C) KH07-02 D42-103 (crossed-nicols): an oxide-gabbro with large orthopyroxene oikocrysts altered, in-part, to brown amphibole, ophitic with large amounts of multi-generational plagioclase. (D) KH07-02 D42-111 (plain polarized light): An oxide-rich gabbro with large clinopyroxene/amphibole oikocrysts ophitic with large amounts of plagioclase.

The ultramafic rocks are serpentinized to variable amounts (35 – 70 vol. %) with harzburgites and dunites generally more altered than wehrlite and gabbro. Lizardite-magnetite mesh texture assemblages commonly replace olivine and bastite replaces pyroxene. Plagioclase often displays variable alteration to phyllosilicates with relict grains preserved as cores with alteration coronas.

The porphyroclastic textures typical of harzburgite tectonites are common in the harzburgites and heavily altered peridotites (herein referred to collectively as harzburgites) of dredge D31 and are characterized by 1-5 mm deformed orthopyroxene porphyroblasts in a matrix of 0.2-0.5 mm serpentinized olivine. In a few samples, round clusters of orthopyroxene and minor spinel show a weak alignment. Spinel ranges from 0.2-1.5 mm in size and anhedral or holly leaf to perfectly euhedral in shape. Although orthopyroxene is present in small amounts as porphyroblasts, very little clinopyroxene is present save for a single clinopyroxene-bearing harzburgite (D31-031). The dunites consist of subhedral to rounded olivine that in most cases is heavily serpentinized. Spinel forms euhedral to round <1mm grains in the olivine matrix.

The wehrlites are dominated by poikilitic textures with 1-5 mm, weakly deformed, anhedral or granular olivine associated with variable amounts of undeformed, optically continuous clinopyroxene (~5-15%) and plagioclase (~2-10%) oikocrysts. Clinopyroxene is mostly found as large (1-8 mm) oikocrysts that enclose olivine and spinel grains and as rare small polycrystalline interstitial clinopyroxene clusters. Plagioclase, where present, is mostly altered to a fine grained, pseudomorphous anhedral lobate blebs (0.5-2 mm) with rare <1 mm relict grains preserved in their cores. Spinel is sparse in the wehrlites, but is generally < 1 mm, round, and associated with olivine.

The gabbros contain sub-equal amounts of clinopyroxene and plagioclase with small

amounts of orthopyroxene and olivine (with the exception of D31-302, which is discussed below). Spinel is minor, but ubiquitous in the gabbros lacking Fe-Ti oxides, and is associated with olivine or plagioclase. Grain sizes are generally heterogeneous and vary between 0.4 and 7 mm for clinopyroxene and 0.2 and 2 mm for plagioclase. Clinopyroxene is generally large (1-10 mm), anhedral to lobate, and sub-ophitic, enclosing numerous plagioclase laths (0.2 mm average size). Where present, orthopyroxene and olivine form small single or polycrystalline clusters interstitial to plagioclase and clinopyroxene. D31-302 (ol-gabbro/pl-wehrlite) is a special case in which plagioclase is found randomly oriented within and between large anhedral clinopyroxene oikocrysts (1 – 8 mm) that enclose rounded olivine and minor orthopyroxene (0.1 – 0.5 mm).

Mineral Chemistry

Spinel

Overall, spinel Cr# $[100 \cdot \text{Cr}/(\text{Cr} + \text{Al})]$ and Mg# $[100 \cdot \text{Mg}/(\text{Mg} + \text{Fe}^{2+})]$ in the samples ranges from ~45-87 and ~22-68 with Al_2O_3 and TiO_2 ranging from ~7 to 30 wt.% and ~0 to 2.25 wt.% respectively (Fig. 5). Overall, (Table 2) major element oxides have standard deviations between 0.01 and 1.69 weight percent. The wide range in standard deviations is an indication of the presence of compositional heterogeneity within some of the spinels.

Table 2: Spinel Major Elements (1 of 2)

Sample	D31-002	D31-004	D31-010	D31-013	D31-020	D31-024	D31-026	D31-101	D31-103	D31-105	D31-106	D31-107
Lithology	Perid.	Harz.	Harz.	Dun/Harz.	Harz.	Dun/Harz.	Dun.	Wehrl.	Pl-wehrl.	Pl-wehrl.	Pl-wehrl.	Ol-gabb.
N	15	13	11	6	13	8	9	19	27	21	5	5
MgO	11.10	11.18	11.44	8.77	10.44	10.20	9.92	13.42	10.89	11.32	9.13	14.96
SiO ₂	0.00	0.00						0.00	0.00			0.04
Al ₂ O ₃	21.20	17.89	17.02	7.14	16.64	12.08	7.85	26.24	24.73	23.67	18.97	29.16
Cr ₂ O ₃	44.46	50.33	49.56	62.88	50.42	58.52	61.75	40.82	38.14	39.16	42.08	38.19
CaO	0.02	0.01						0.01	0.02			0.05
TiO ₂	0.19	0.10	0.01	0.06	0.01	0.01	0.08	0.07	0.13	0.20	0.52	0.07
MnO	0.24	0.22	0.21	0.28	0.20	0.22	0.25	0.17	0.22	0.20	0.28	0.17
FeO*	21.95	19.79	20.95	20.80	22.05	18.93	19.48	18.86	24.92	24.42	27.43	16.98
FeO	17.94	17.29	16.81	19.54	18.48	18.14	17.76	15.29	18.80	18.18	20.82	13.39
Fe ₂ O ₃	4.45	2.78	4.60	1.40	3.97	0.88	1.92	3.96	6.80	6.93	7.34	3.98
NiO	0.09	0.06	0.10	0.04	0.08	0.05	0.04	0.08	0.12	0.12	0.12	0.15
V ₂ O ₃	0.11	0.16						0.13	0.15			0.11
ZnO	0.19	0.17						0.17	0.16			0.03
Total	100.01	100.20	99.29	99.96	99.83	100.03	99.37	100.36	100.16	99.08	98.52	100.31
Cr#	58.48	65.31	67.21	86.11	68.08	77.32	84.70	51.08	50.91	53.79	60.96	46.77
Mg#	52.43	53.53	49.32	42.90	45.71	49.00	47.57	61.00	50.81	45.23	37.26	66.57

Table 2: Spinel major and minor element concentrations from EMPA at Texas A&M University and the University of Houston. Error is reported as an average of the standard deviations for each oxide in each sample (next page).

Table 2: Spinel Major Elements (2 of 2)

Sample	D31-301	D31-302	D42-101c	D31-021a	D31-015	D31-025	D31-022	D31-031	D31-026a	D31-012		
Lithology	Cpxnt.	Ol-gabb.	Dun.	Dun.	Perid.	Dun.	Dun.	Cpx-Harz.	Dun.	Cpxnt.	Average	Mean σ (wt.%)
N	3	11	9	10	20	22	11	14	8	9		
MgO	3.39	4.70	12.33	12.93	6.41	11.39	10.00	11.50	9.30	6.19	11.06	0.51
SiO ₂	0.01	1.21		0.09	0.02	0.05	0.05	0.06	0.02	0.01	0.01	0.26
Al ₂ O ₃	0.02	13.40	20.80	20.54	10.84	9.66	10.60	15.20	8.06	9.74	18.55	0.86
Cr ₂ O ₃	0.15	31.61	47.35	47.74	45.10	61.26	59.69	56.02	61.65	57.33	48.03	0.83
CaO	0.02	0.06		0.00	0.00	0.00	0.01	0.00	0.00	0.00	0.02	0.01
TiO ₂	53.03	2.06	0.13	0.13	0.04	0.08	0.06	0.01	0.08	0.09	0.12	0.02
MnO	1.80	0.36	0.19	0.44	0.59	0.47	0.51	0.45	0.52	0.55	0.22	0.04
FeO*	41.86	44.53	19.34	19.46	36.47	18.09	20.37	18.26	21.54	26.62	21.38	1.26
FeO	41.86	27.59	16.45	15.71	24.36	16.09	18.31	16.88	19.01	23.71	17.70	0.97
Fe ₂ O ₃	0.00	18.83	3.22	4.17	13.46	2.23	2.28	1.53	2.82	3.24	4.08	0.77
NiO	0.03	0.20	0.10	0.09	0.21	0.04	0.03	0.04	0.06	0.06	0.09	0.03
V ₂ O ₃	0.16	0.64									0.13	0.02
ZnO	0.01	0.20		0.10	0.17	0.15	0.18	0.20	0.13	0.28	0.15	0.06
Total	100.48	100.85	100.25	101.52	99.86	101.21	101.50	101.73	101.36	100.87	99.76	
Cr#	83.82	61.28	61.56	60.93	76.05	80.97	79.07	71.20	83.69	79.82	64.23	
Mg#	12.61	23.28	53.18	54.22	25.80	52.89	46.67	52.90	43.49	29.25	50.11	

Table 2: Spinel major and minor element concentrations from EMPA at Texas A&M University and the University of Houston. Error is reported as an average of the standard deviations for each oxide in each sample.

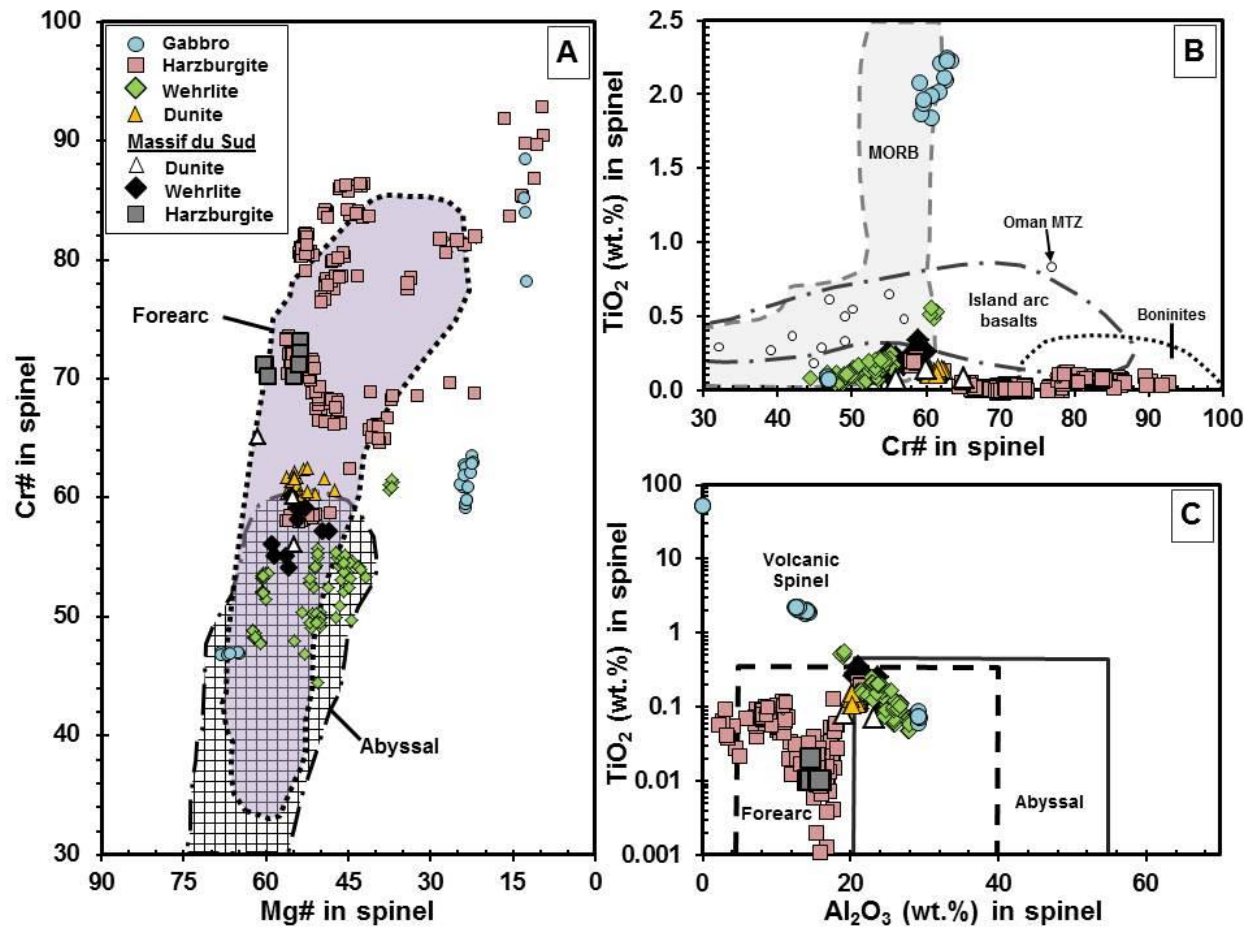


Figure 5: (A) Spinel Cr# vs Mg#. (B) Spinel Cr# vs TiO₂ (wt. %). Data for MORB, Oman mantle transition zone, Island Arc Basalts, and Boninites from Arai (1992), Koga et al., (2001), Kelemen et al., (1995), and Dick and Natland (1996) respectively. (C) Spinel Al₂O₃ (wt. %) vs TiO₂ (wt. %) based on Kamenetsky et al. (2001). Fields for forearc and abyssal peridotites from (Dick and Bullen, 1984). Massif du Sud ophiolite data from Marchesi et al. (2009) and Godzilla Megamullion data is from Sanfilippo et al. (2013). The Massif du Sud ophiolite, New Caledonia, is a comparable sample suite in that they represent a more recent forearc associated with the same Western Pacific tectonic setting as dredge D31.

Two distinct groups of samples have been identified based on the Cr#, Al₂O₃, and TiO₂ contents of their spinels (Fig. 5), group M and group B. Group M spinels are medium in Cr# (~45-60) and are overall higher in Al₂O₃ (19 to 29 wt. %) and TiO₂ (0.1 to 2.25 wt. %). Group B spinels are high in Cr# (65 to 87) and are overall lower in Al₂O₃ (8 to 20 wt. %) and TiO₂ (0 to 0.1 wt. %). Relative variations of Al₂O₃ versus TiO₂ can be used to characterize spinels as volcanic, abyssal, or arc related (Kamenetsky et al., 2001). Group M spinels plot mostly in the field of abyssal peridotite spinels with a trend moving towards arc-like and volcanic spinels, while group B spinels plot entirely within the field of arc-like spinels (Fig. 5c). Samples that fall into group M consist of plagioclase-bearing peridotites, wehrlites, gabbros, and 1 cpx-harzburgite, whereas group B samples consist of only peridotites and dunites (See Table 2).

Olivine

Major element analysis of olivines (Table 3) found overall ranges in forsterite content from Fo_{82.4} to Fo_{92.5} and NiO and MnO from 0.18 to 0.45 and 0.08 to 0.25 wt. % respectively. Olivines in the ‘gabbroic’ rocks have compositions of Fo_{82.4} to Fo_{83.6} with NiO and MnO ranging from 0.18 to 0.31 and 0.21 to 0.25 wt. % respectively. Olivines from the peridotites or ‘harzburgite’ group have compositions of Fo_{91.2-92.5} with NiO and MnO ranging from 0.37-0.45 (abyssal peridotites average 0.3 wt. %; Sanfilippo et al., 2013) and 0.08-0.14 wt. % respectively. Olivines from the ‘wehrlitic’ rocks have compositions of Fo_{90-91.6} with NiO and MnO ranging from 0.18-0.31 and 0.11-0.17 wt. % respectively (Fig. 6). Note that there is no significant overlap between olivine compositions in the gabbros with the wehrlites and harzburgites, but there is minor overlap between the wehrlites and harzburgites with the wehrlites trending towards more depleted compositions.

Table 3: Olivine Major Elements

Analysis	D31-004	D31-105	D31-301	D31-101	D31-103	D31-302		
Lithology	Harz.	Pl-wehrl.	Dun/Cpxnt.	Wehrl.	Pl-wehrl.	Ol-gabb.	Average	Mean σ (wt.%)
N	14	5	4	10	8	10		
MgO	51.53	49.97	45.24	50.23	50.07	44.87	48.65	0.23
SiO ₂	41.63	41.01	39.91	41.58	41.03	39.75	40.82	0.20
Al ₂ O ₃	0.00	0.04	0.01	0.05	0.01	0.01	0.02	0.01
CaO	0.02	0.11	0.03	0.33	0.05	0.03	0.10	0.05
TiO ₂	0.00	0.01	0.01	0.01	0.00	0.02	0.01	0.01
MnO	0.12	0.15	0.24	0.13	0.15	0.23	0.17	0.01
FeO	8.15	9.52	15.90	9.17	9.57	16.15	11.41	0.17
NiO	0.42	0.29	0.22	0.23	0.28	0.29	0.29	0.03
Total	101.87	101.09	101.55	101.73	101.16	101.35	101.46	
Fo	91.77	90.34	83.36	90.98	90.25	83.03	88.29	

Table 3: Olivine major and minor element concentrations from EMPA at Texas A&M University and the University of Houston. Error is reported as an average of the standard deviations for each oxide in each sample .

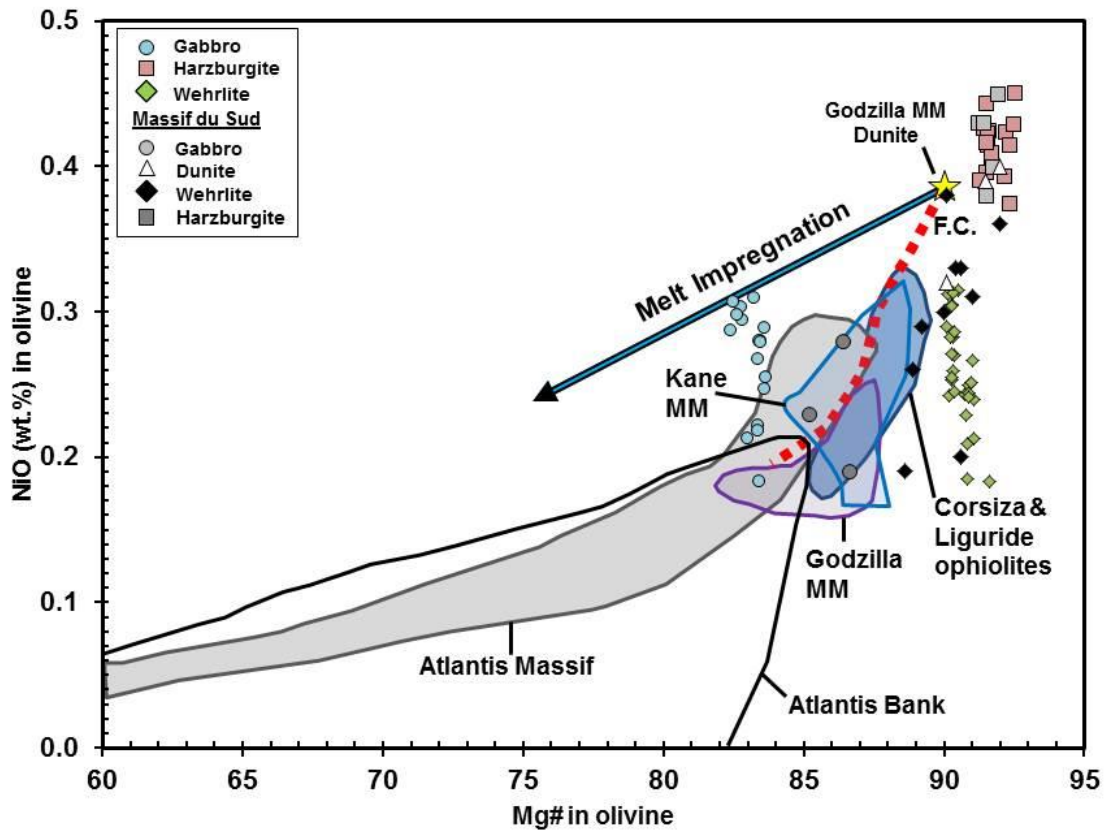


Figure 6: Mg# or Forsterite content (Fo) in olivine versus NiO (wt. %) for electron microprobe analyses of olivine from dredge D31 peridotites. The fractional crystallization curve (F.C.) and Godzilla Megamullion data are from Sanfilippo et al. (2013). Comparison data are as follows: Atlantis Massif (Suhr et al., 2008; Drouin et al., 2009), Kane Megamullion (Dick et al., 2010), Corsica and Liguria ophiolites (Renna and Tribuzio, 2011; Sanfilippo, 2011; Sandfilippo and Tribuzio, 2012).

Pyroxene

Most major element analyses of pyroxenes (Table 4) are for clinopyroxene due to the scarcity of orthopyroxene, and a lack of grains suitable for analysis. Overall clinopyroxene Mg#s extend from 86.1 to 97.96, with significant diversity between lithologies (Figures 7 and 8). By

lithology, Mg# ranges from 86.1-94, 92.4-92.98, and 93.86-97.96 in the gabbros, harzburgites, and wehrlites respectively. TiO_2 and Na_2O contents range from 0.03-0.17 and 0.1-0.21 in the gabbros, below detection limits – 0.02 and 0.03 in the harzburgites, and 0.01 – 0.11 and 0.01-0.25 in the wehrlites. Al_2O_3 and Cr_2O_3 contents of the clinopyroxenes range from 8.2-3.98 and 0.95-1.35 in the gabbros, 1.06-1.16 and 0.50-0.58 in the harzburgites, and 0.15-4.21 and below detection limits to 1.61 in the wehrlites. CaO in the clinopyroxenes covers a wide range of compositions from 14.08-22.87 in the gabbros, 0.64-1.06 in the harzburgites, and 13.14-25.75 in the wehrlites. The clinopyroxene composition in the harzburgites overlaps in part with the gabbros and generally plots between the wehrlites and gabbros.

Table 4: Pyroxene Major Elements

Analysis	D31-105	D31-107	D31-301	D31-101	D31-103	D31-031	D31-108				D31-004	D31-301	D31-302		
Lithology	Pl-wehrl.	Ol-gabb.	Dun/Cpxnt.	Wehrl.	Pl-wehrl.	Cpx-Harz.	Gabbro		Mean σ		Harz.	Dun/Cpxnt.	Ol-gabb.		Mean σ
Grain	Cpx	Cpx	Cpx	Cpx	Cpx	Cpx	Cpx	Average	(wt.%)		Opx	Opx	Opx	Average	(wt.%)
N	4	9	4	11	9	9	6				5	4	4		
Na ₂ O	0.01	0.13	0.17	0.12	0.13	0.01	0.14	0.10	0.02		0.02	0.02	0.01	0.01	0.01
MgO	18.21	18.01	19.77	17.81	17.15	35.00	18.22	20.60	0.42		34.81	30.51	30.71	32.01	0.34
SiO ₂	54.94	52.21	52.35	51.97	52.62	57.29	53.04	53.49	0.28		57.84	54.93	55.25	56.00	0.19
Al ₂ O ₃	0.26	3.82	3.45	4.07	3.00	1.12	3.74	2.78	0.19		1.06	2.85	1.74	1.89	0.11
Cr ₂ O ₃	0.00	1.18	1.08	1.43	1.10	0.53	1.20	0.93	0.12		0.46	0.58	0.39	0.48	0.03
CaO	25.11	22.23	17.63	22.19	23.90	0.82	22.62	19.22	0.70		1.33	1.05	1.14	1.17	0.56
TiO ₂	0.01	0.07	0.15	0.07	0.08	0.00	0.06	0.06	0.01		0.01	0.07	0.23	0.10	0.01
MnO	0.06	0.06	0.11	0.04	0.06	0.16	0.09	0.09	0.02		0.14	0.19	0.23	0.19	0.02
FeO	0.95	1.25	4.01	1.41	1.13	4.93	2.82	2.36	0.36		5.18	9.72	9.78	8.23	0.30
Fe ₂ O ₃	1.03	1.81	1.65	1.65	1.48			1.52	0.36		0.31	0.54	0.88	0.58	0.27
NiO						0.04	0.05	0.05	0.04						
Total	100.59	100.76	100.36	100.77	100.66	99.90	102.00	100.72	0.37		101.16	100.45	100.37	100.66	0.35
Mg#	97.17	96.26	89.77	95.76	96.44	92.68	92.00	94.30			92.30	84.84	84.85	87.33	0.37

Table 4: Clinopyroxene and Orthopyroxene major and minor element concentrations from EMPA at Texas A&M University and the University of Houston. Error is reported as an average of the standard deviations for each oxide in each sample.

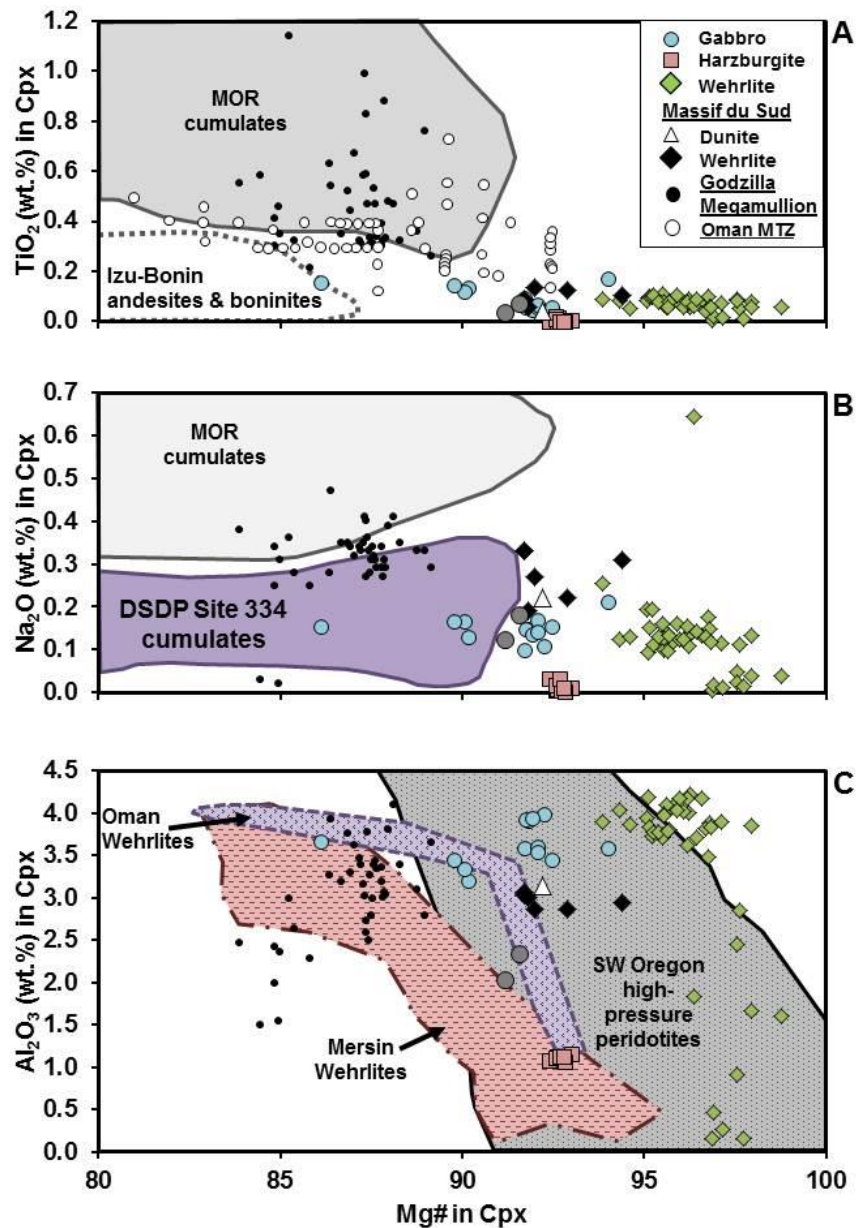


Figure 7: Mg# vs (A) TiO₂ (wt. %), (B) Na₂O (wt. %), and (C) Al₂O₃ (wt.%). Fields for MOR cumulates, Izu-Bonin andesites and boninites, Oman MTZ, DSDP Site 334 cumulates, Oman wehrlites, Mersin wehrlites, and SW Oregon high-pressure peridotites are from Ross and Elthon (1993), Nonnotte et al. (2005), Koga et al. (2001), Ross and Elthon (1993), Koga et al. (2001), Parlak et al. (1996), and Medaris et al. (1972) respectively.

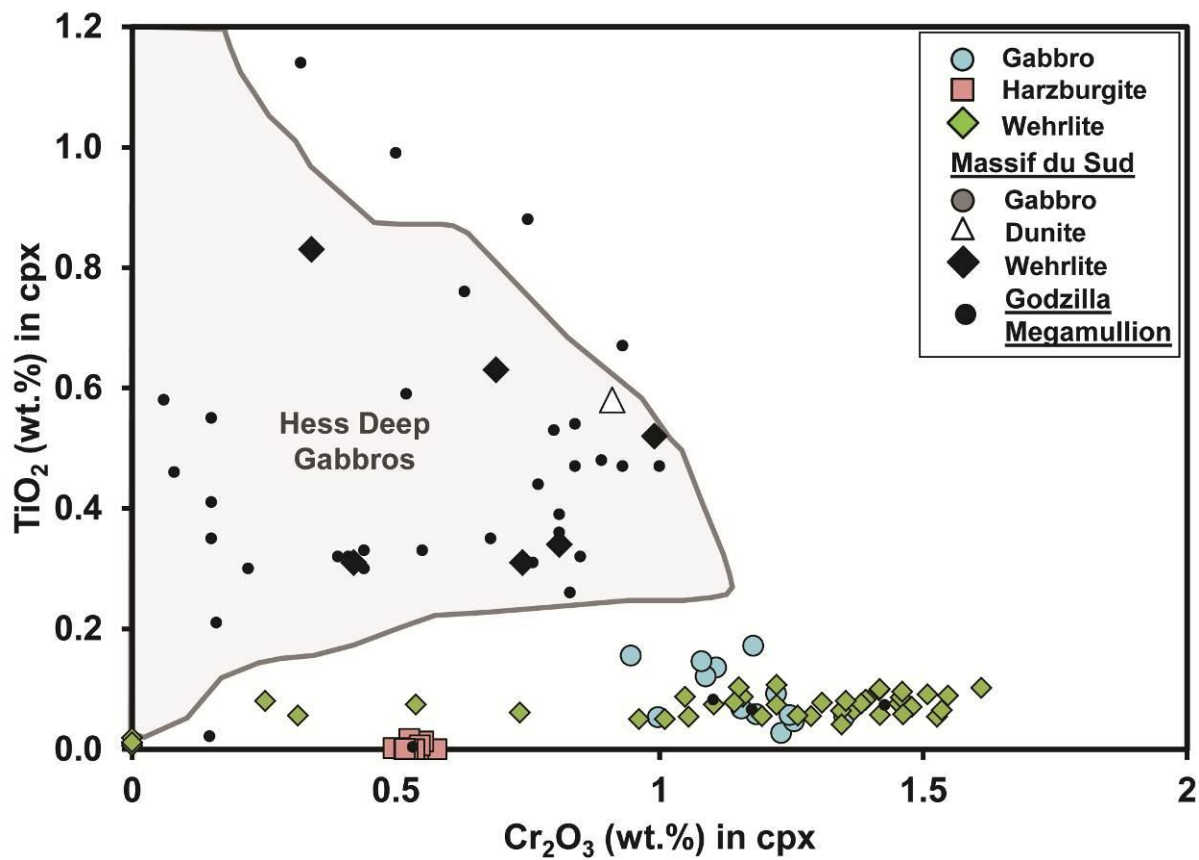


Figure 8: Cr_2O_3 (wt. %) vs TiO_2 (wt. %) in clinopyroxene. Hess Deep Gabbros and Godzilla Megamullion data come from Lissenberg et al. (in press) and Sanfilippo et al. (2013).

The few orthopyroxenes that were analyzed are from D31-004 (a protogranular, relatively fresh harzburgite with noticeable amounts of clinopyroxene), D31-301 (a >1.5 cm large clinopyroxene with orthopyroxene exsolution in reactive contact with a dunite), and D31-302 (a sub-ophitic gabbro with very rare, small, orthopyroxene exsolution lamella within clinopyroxene). The range in chemistries of orthopyroxene shows little to no overlap between ‘gabbros’ and harzburgites. Mg# ranges from 84.4 to 85.2 in the gabbro and 91.8 to 93.1 in the harzburgite. TiO_2 ranges from below detection limits to 0.25 and 0.02 in the gabbros and harzburgites respectively. Al_2O_3 and Cr_2O_3 range from 1.69 to 3.06 and 0.36 to 0.61 and 0.97-1.13 for the gabbro and 0.4-0.51 for the harzburgite.

Trace Element Geochemistry

Chondrite normalized REE patterns for D31 clinopyroxenes are plotted in Figure 9 based on analyses from Table 5. Included in this diagram are fields of boninitic cumulates (Tribuzio et al., 2008), DSDP 334 depleted cumulates (Nonnotte et al., 2005), Oman and Kohistan mantle transition zone rocks (Kelemen et al., 1997; Koga et al., 2001; Garrido et al., 2007), and rocks from the Massif du Sud ophiolite mantle transition zone (Marchesi et al., 2009) for comparison. Overall, the samples have highly depleted REE patterns with somewhat low MREE to HREE ratios and LREE depletions. All samples follow the same relative trend in slight HREE enrichment and heavy LREE depletion regardless of lithology, with the major difference being that the gabbros show a slightly higher enrichment in HREEs. The presence of a La enrichment relative to Ce in most of the samples is considered to be due to contamination and not related to the actual composition of the clinopyroxenes.

Table 5: LA-ICP-MS analyses of clinopyroxene

n	D31-301		D31-101		D31-103		D31-107		Standards		Normalizing Value
	Grain 1	Grain 2	Grain 1	Grain 2	Grain 1	Grain 2	Grain 1	Grain 2	KL2-G ^A	ATHO-G ^B	Cl-Chondrite ^C
	5	3	4	4	4	4	4	3	18	10	
Li	3.868	1.411	0.692	1.681	2.033	1.759	0.323	0.738	5.1	28.6	1.6
Be	0.171	0.025	0.260	0.000	0.184	0.118	0.264	0.366	0.88	3.2	0.03
B	0.345	0.297	0.336	0.297	0.894	0.535	0.426	0.331	2.73	5.7	0.3
Sc	69.099	68.443	66.751	66.608	78.112	78.061	71.781	70.764	31.8	7	5.9
Ti	767.620	823.728	325.523	428.147	505.808	579.581	300.920	296.676	15343	1528	630
V	243.445	242.097	232.541	262.150	244.910	232.372	181.455	180.724	309	3.91	56
Mn	994.471	926.141	612.556	624.371	783.172	713.703	595.768	583.958	1277.8	820.95	1920
Co	39.602	33.264	30.703	30.196	42.925	36.605	30.470	30.709	41.2	2.13	501
Ni	410.610	344.573	282.069	256.219	559.391	523.418	291.542	298.488	112	13	10700
Cu	17.035	8.631	1.173	1.426	1.913	1.588	2.098	3.688	87.9	18.6	120
Zn	28.993	21.332	14.670	18.381	21.471	17.201	14.623	11.492	110	141	312
Ga	5.216	3.692	2.918	3.410	3.792	3.638	3.068	3.195	20	25.3	9.2
Rb	0.272	0.139	0.238	0.209	0.168	0.228	0.196	0.247	8.7	65.3	2.3
Sr	2.167	2.167	2.411	3.426	4.783	3.775	1.764	1.764	356	94.1	7.25
Y	5.305	5.393	1.681	2.284	2.938	3.143	1.764	1.717	25.4	94.5	1.57
Zr	1.059	1.361	0.401	0.510	0.518	0.898	0.154	0.125	152	512	3.82
Nb	0.017	0.026	0.026	0.021	0.029	0.027	0.025	0.032	15	62.4	0.24
Cs	0.024	0.011	0.030	0.017	0.008	0.022	0.023	0.014	0.115	1.08	0.19
Ba	0.392	0.231	0.351	0.327	0.760	0.356	0.255	0.157	123	547	3.45
La	0.035	0.022	0.011	0.018	0.035	0.060	0.013	0.010	13.1	55.6	0.24
Ce	0.114	0.138	0.036	0.052	0.060	0.090	0.029	0.020	32.9	121	0.61
Pr	0.033	0.039	0.019	0.026	0.023	0.035	0.011	0.023	4.6	14.6	0.09
Nd	0.373	0.384	0.110	0.225	0.201	0.227	0.103	0.095	21.7	60.9	0.46
Sm	0.248	0.253	0.131	0.163	0.138	0.174	0.111	0.090	5.55	14.2	0.15
Eu	0.134	0.093	0.053	0.046	0.072	0.081	0.053	0.051	1.92	2.76	0.06
Gd	0.528	0.564	0.198	0.328	0.262	0.350	0.206	0.189	5.92	15.3	0.2
Tb	0.110	0.119	0.049	0.048	0.059	0.065	0.040	0.049	0.89	2.51	0.04
Dy	0.966	0.854	0.311	0.415	0.443	0.537	0.329	0.264	5.22	16.2	0.25
Ho	0.203	0.201	0.069	0.082	0.091	0.116	0.075	0.068	0.961	3.43	0.06
Er	0.679	0.603	0.209	0.251	0.353	0.359	0.221	0.231	2.54	10.3	0.16
Tm	0.102	0.107	0.027	0.057	0.064	0.057	0.039	0.049	0.331	1.52	0.02
Yb	0.691	0.658	0.261	0.309	0.370	0.415	0.250	0.225	2.1	10.5	0.16
Lu	0.085	0.103	0.038	0.038	0.062	0.047	0.053	0.045	0.285	1.54	0.02
Hf	0.132	0.078	0.041	0.068	0.073	0.058	0.036	0.053	3.93	13.7	0.1
Ta	0.014	0.007	0.016	0.020	0.012	0.026	0.018	0.018	0.961	3.9	0.01
Pb	0.065	0.039	0.053	0.033	0.065	0.050	0.058	0.051	2.07	5.67	2.47
Th	0.024	0.025	0.016	0.025	0.027	0.019	0.025	0.039	1.03	7.4	0.03
U	0.026	0.026	0.020	0.026	0.214	0.159	0.023	0.034	0.548	2.37	0.07

^A Jochum, K.P. (2006)^B Icelandic Rhyolite Glass^C McDonough and Sun, 1995

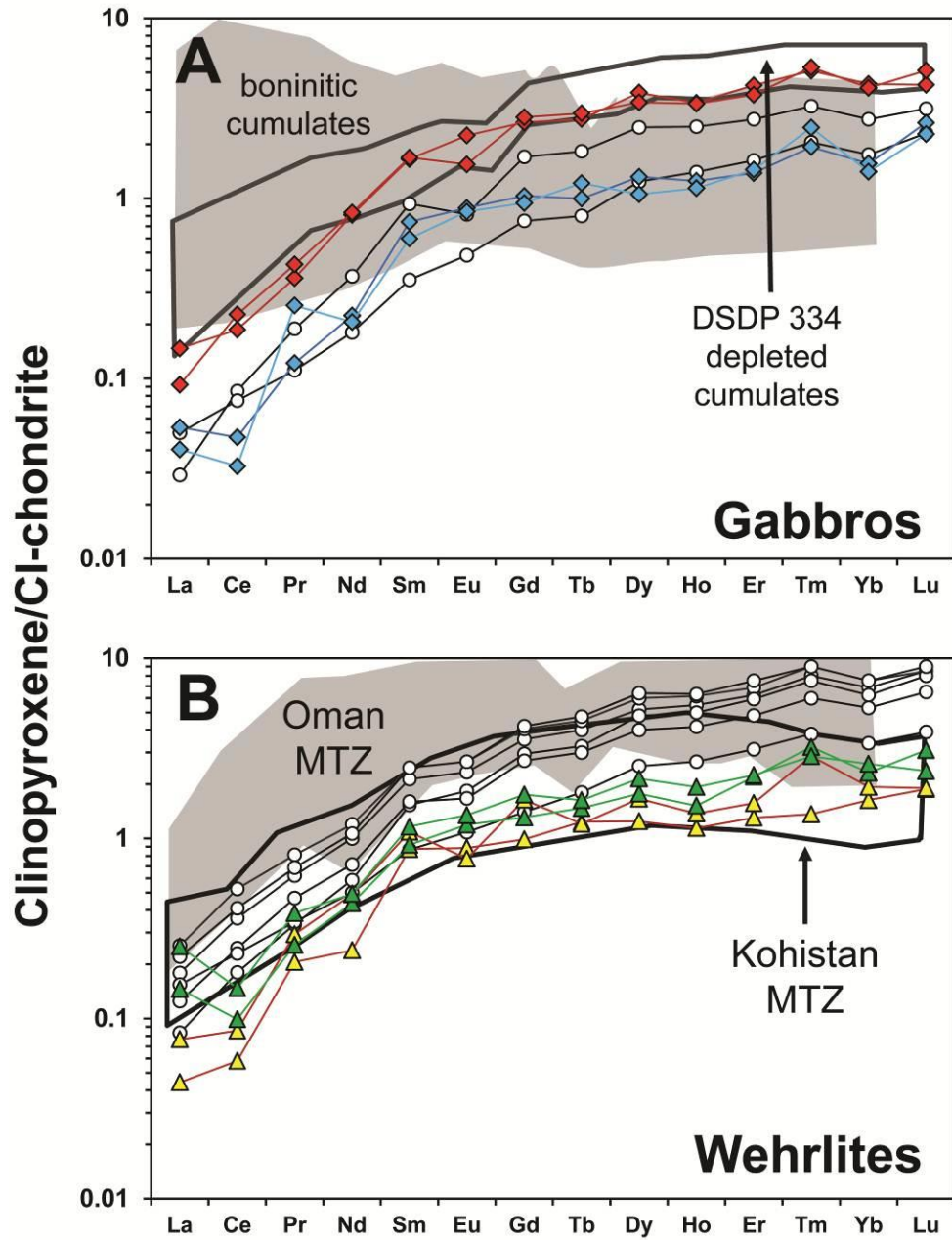


Figure 9: CI-chondrite normalized (Workman and Hart, 2005) REE plots for D31 clinopyroxenes from gabbros and wehrlites compared against Massif du Sud clinopyroxenes (white circles) (Marchesi et al. (2009)). Fields for Boninitic cumulates, DSDP 334 cumulates, Oman MTZ, and Kohistan MTZ come from Tribuzio et al. (2008), Nonnotte et al. (2005), Koga et al. (2001), and Garrido et al. (2007) respectively.

DISCUSSION

Melt Stagnation and Melt-Rock Reaction in the Lower Crust

Interactions between transient MORB melts and mantle rocks commonly result in the formation of replacive dunites and plagioclase-impregnated peridotites (e.g.: Dick, 1977; Quick, 1981; Bonatti et al., 1992; Kelemen and Dick, 1995; Dick and Natland, 1996; Rampone et al., 1997; Tartarotti et al., 2002; Sanfilippo et al., 2013). It has been shown that more extensive melt-rock interaction in the mantle (e.g. larger volumes of melt) can lead to the formation of ‘hybridized’ gabbros and troctolites which incorporate a large amount of mantle-derived minerals (Dick and Natland, Sci Res. 1996; Kelemen et al., 2004; Sanfilippo et al., 2013). Such processes have been documented in olivine-rich troctolites and impregnated harzburgites (Tamura et al., 2008; Godard et al., 2009; Sanfilippo and Tribuzio, 2012), the mantle transition zone at Kane Megamullion (Dick et al., 2010) from the lower crust drilled at the Atlantis Massif, Mid-Atlantic Ridge (Drouin et al., 2007, 2009; Suhr et al., 2008) and in ophiolites such as the Ligurians (Renna and Tribuzio, 2011). The cases involving olivine-rich troctolites are thought to have formed from crystallizing MORB melts which stagnated during migration through partial dissolution of replacive dunite in mantle conduits and stagnation zones at the crust-mantle transition with precipitation of plagioclase and minor Cpx.

If a melt is reacted with a large enough mass of enclosing mantle material, effectively lowering the bulk solidus below that of ambient temperature, the stagnated melt can undergo complete and isothermal solidification (Dick and Natland, 1996; Dick et al., 2010; Sanfilippo et al., 2013). Mimicking the liquid line of descent of MORB melt undergoing equilibrium or fractional crystallization, but at higher Mg#, the sequence of crystallization causes an undersaturation of olivine in the liquid (Arai and Matsukage, 1996; Dick and Natland, 1996;

Sanfilippo et al., 2013). This leads to the corrosion of olivine and precipitation of plagioclase \pm clinopyroxene, which is basically a reversal in the formative textures of replacive dunites. The resulting formation of plagioclase impregnated peridotite due to shallow mantle melt infiltration in the shallow mantle is considered a classic example of this process (Dick and Bullen, 1984; Rampone et al., 1997; Tartarotti et al., 2002; Piccardo et al., 2006; Brunelli and Seyler, 2010; Dick et al., 2010). This process is commonly associated in the crust/mantle transition with characteristically abundant troctolite, wehrlite, dunite, and clinopyroxene \pm plagioclase dunite which commonly characterize the crust/mantle transition (Nicolas and Prinzhofer, 1983; Boudier and Nicolas, 1995; Sanfilippo et al., 2013).

The textures observed in the wehrlites, plagioclase-bearing peridotites, and gabbros of dredge D31 indicate an origin related to progressive melt-infiltration and stagnation. Anhedral, polygonal to rounded olivine grains within the D31 wehrlites, in many cases embayed by clinopyroxene, exhibit signs of chemical disequilibrium with infiltrating melt (Fig. 4b). In many cases, the olivine seems to have been in the process of being resorbed during clinopyroxene crystallization. In some of the wehrlites, both clinopyroxene and plagioclase are present as an infiltrating phase. In some samples they intermingle with sharp contacts, while other samples contain discreet zones of clinopyroxene or plagioclase with relatively sharp contacts. Both cases suggest that neither plagioclase nor clinopyroxene was reacting with the melt during crystallization. Along with the solely oikocrystic nature of clinopyroxene compared to the olivine and plagioclase, these features suggest that the melt infiltrated into an olivine matrix and was initially saturated in plagioclase (Sanfilippo et al., 2013). These textures are very similar to those of olivine-rich troctolites from the Mid-Atlantic Ridge and the Godzilla Megamullion (Lissenberg and Dick, 2008; Suhr et al., 2008; Drouin et al., 2009, 2010; Dick et al., 2010;

Sanfilippo et al., 2013).

Similar to rocks studied by Sanfilippo et al. (2013) from the Godzilla Megamullion, dredge D31 clinopyroxenes have higher Mg#s than expected for MORB crystallized at low pressures (Tormey et al., 1987; Grove et al., 1990,1992; Yang et al., 1996). The stability field for MORB clinopyroxene is shown in experimental data to expand with increasing pressure to a point where clinopyroxene preferentially crystallizes out prior to olivine and plagioclase (Presnall et al., 1978; Grove et al., 1992). This is why high-Mg# clinopyroxenes are generally thought to indicate high pressure crystallization (Elthon et al., 1982). It must also be noted, that the addition of water to a melt can accommodate clinopyroxene crystallization before plagioclase and olivine (Feig et al., 2006 and references therein). However, high-Mg# clinopyroxene can also be produced by either subsolidus equilibration of interstitial melt-derived clinopyroxene with cumulus olivine (Meyer et al., 1989) or the crystallization of clinopyroxene from migrating melt which is resorbing high-Fo olivine (Dick and Natland, 1996; Bedard et al., 2000; Kvassnes, 2004; Kvassnes and Grove, 2008; Lissenberg and Dick, 2008).

Although the textures and Mg#s of the D31 clinopyroxenes suggest a magmatic origin, the low-TiO₂ and high-Cr₂O₃ content of the clinopyroxenes suggest that they are not the product of fractional crystallization of a MORB liquid. Estimates of Cr₂O₃ contents of melts in equilibrium with D31 clinopyroxenes (using a partition coefficient of 3.8 from Hart and Dunn, 1993) suggest melt Cr concentrations ranging from 1750 – 3200 ppm. This is far in excess of what is considered reasonable for MORB compositions (Roeder and Reynolds, 1991). Assimilation of chromian diopside from adjoining wall rock peridotite during the formation of replacive dunites can reasonably account for the localized formation of a high-Cr melt (Dick, 1977; Quick, 1981). This would cause the Cr# of spinel in olivine- and plagioclase-saturated

MORB and abyssal dunites to gradually increase with the decrease in olivine or melt Mg# (Dick and Bullen, 1984). The co-precipitation of both clinopyroxene and spinel will drastically decrease the Cr# of the melt leading to large ranges in the Cr contents of the phases and eventually terminate spinel crystallization.

We infer that the wehrlites and primitive plagioclase-poor gabbros (i.e. mela-gabbros) of dredge D31 represent the progressive crystallization and reaction of percolating melt with the matrix and wall-rock of melt-transport conduits. Progressive reaction and crystallization of subsequent melts leads to the further development of clinopyroxene-rich rocks and eventually more plagioclase-rich rocks at the periphery of such conduits. This leads to the re-working of previously reacted material (i.e. wehrlites and pl-wehrlites) and development of more evolved rocks such as primitive gabbros. Such wehrlitic/troctolitic and gabbroic segregations associated with dunites with similar textures have been identified in lower crustal sections along the Mid-Atlantic Ridge (Lissenberg and Dick, 2008; Suhr et al., 2008; Drouin et al., 2009, 2010; Dick et al., 2010), at Hess Deep (Dick and Natland, 1996) and at the Godzilla Megamullion (Sanfilippo et al., 2013). Based on the wide range of localities where these characteristic assemblages have been observed, it is generally agreed that shallow melt-rock reaction and melt stagnation is ubiquitous across the spreading rate spectrum and tectonic environments.

Overall, a possible gradation can be found in a number of the samples that seems to follow a path of increasing addition of melt from dunite/harzburgite → wehrlite → plagioclase-wehrlite → olivine-gabbro. This gradation from residual peridotite to more primitive gabbro is characteristic of the addition and reaction of melt into a residual peridotite at varying melt fractions (Lissenberg and Dick, 2008; Suhr et al., 2008; Drouin et al., 2009; Dick et al., 2010; Sanfilippo et al., 2013). This mechanism for the creation of the wehrlites is supported by the

observation of classic cumulate and poikilitic textures including the change from wehrlitic/troctolitic segregations within peridotite to peridotitic segregations within wehlrite (Fig. 4 and 10). This pattern of melt addition seemingly continues in the plagioclase-wehrlites and more plagioclase-rich primitive gabbros (i.e. plagioclase-wehlrite → olivine-gabbro/gabbro). The same cumulate textures are exhibited within the orthopyroxene-bearing olivine-gabbro and begins to even include ophitic to sub-ophitic relationships which would indicate possible active processes of cumulate recycling (Sanfilippo et al., 2013, and references there in). These same relationships have been described in drill cores from Hess Deep (Dick and Natland, 1996; Natland and Dick, 1996) and lower crustal units of ophiolites (Ramp, 1961; Savel'yeva et al., 1980; Boudier and Coleman, 1981; Quick, 1981; Nicolas and Violette, 1982; Ceuleneer and Nicolas, 1985; Nicolas, 1989; MacLeod and Yaouanq, 2000; Marchesi et al., 2009).

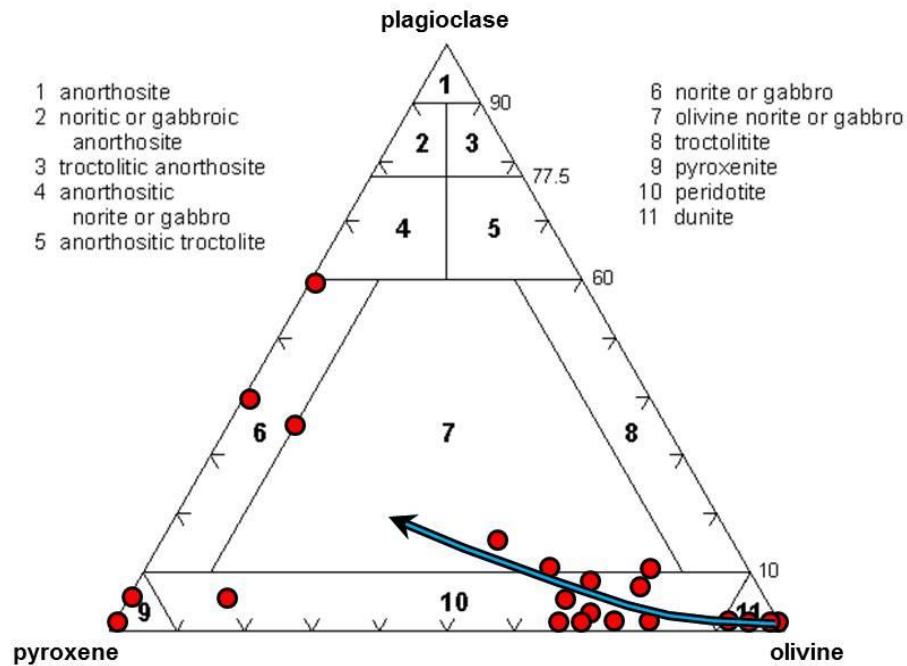


Figure 10: Estimated modal abundances for D31 lower crustal rocks projected onto the combined ultramafic/mafic classification ternary of Streckeisen (1967). The general trend of the D31 lithologies follows roughly that of crust-mantle transition zones reported by previous studies (e.g. Dick and Natland, 1996; Kelemen et al., 1995; Kelemen et al., 1997; Korenaga and Kelemen, 1998; Morishita et al., 2011b). The arrow follows the trend from the center of dunite conduits outward towards the edges where reaction with stagnated melt has crystallized out clinopyroxene and small amounts of plagioclase (with possible orthopyroxene) in wehrlites and possibly pyroxenites. As you move out from the conduit and into the lower crustal plutonic rocks, there is an increase in plagioclase and a marked increase in clinopyroxene up into proper gabbros. Note the lack of rocks containing transitional amounts of olivine (olivine gabbros) between the proper wehrlites and gabbros.

Contrasting MORB-Boninite Reaction Trends in the Bonin Ridge Lower Crustal Spinels

Analysis of spinels from dredge D31 rocks has revealed two chemically distinct and contrasting trends. Group M consists of plagioclase-bearing rocks and Group B consists of solely plagioclase-free, and in some cases pyroxene-poor, peridotites and dunites. Similar groupings to those in this study have been found in spinels from peridotites recovered by the ROV KAIKO7000II from dive site 7K417 that were determined to occur in close proximity to one another (Morishita et al., 2011b). Dive 7K417 followed roughly the same path as dredge D31 (see Figure 3), and serves as a reference for the locations and spatial relationships of samples and lithologies recovered by the dredge. Based on the chemical systematics and lithologic distributions reported by Morishita et al. (2011b), we infer that D31 samples of group M and group B might occur in a similar manner in outcrop. As is seen in the 7K417 samples and crust/mantle sections in ophiolites, the dunites of dredge 31 might have occurred in outcrop on the slope as networks and veins within pyroxene-bearing peridotite and/or gabbroic rocks (Kelemen et al., 1990; Morishita et al., 2011b).

Parkinson and Pearce (1998) estimated the oxidation conditions of peridotites recovered from serpentine seamounts in the IBM forearc and found that both the oxidized harzburgites and dunites of the Torishima Seamount formed in an arc environment while oxidized dunites and reduced harzburgites from the Conical Seamount were formed under arc and MORB-like conditions respectively. Spinels from the group B samples have Cr#s which exceed those of most abyssal peridotite spinels and are consistent with compositions of spinels that have been found in equilibrium with a boninitic melt (e.g. Danyushevsky et al., 1995; Maehara and Maeda, 2004) (see Figure 5) and in forearc peridotites (Ishii et al., 1992; Morishita et al., 2011b). The group M spinels fall within the most depleted range of abyssal peridotite Cr#s and follow the same trend

in Cr# versus TiO₂ space as those of melt-rock reacted abyssal peridotites collected from mid-ocean ridges (Dick and Bullen, 1984; Dick, 1989; Arai, 1992). This trend is created through the reaction of a depleted abyssal peridotite with a MORB-like tholeiitic melt (Fig. 5). These distinctly different spinel compositions provide evidence for melt-rock reaction in the presence of two contrasting melt compositions within a short distance of one another.

Dating boninite volcanics of the Bonin Ridge shows ages ranging from ~44 to 48 Ma, while dating of the FABs, which have a MORB-like composition, gives an age range of ~50 to 52 Ma (Ishizuka et al., 2011). The presence of this age gap between boninitic and tholeiitic volcanism implies that the reactions that formed the group M and B spinels likely did not occur simultaneously. This suggests that the group M and group B lower crustal rocks are the result of two distinct melt-rock interaction events that are geochemically associated with the transition from the 50-52 Ma FAB volcanism to the 44-48 Ma boninite volcanism, respectively. The lower-crustal and mantle rocks of the Bonin Ridge thus preserve a record of subduction initiation and the early evolution of the Izu-Bonin magmatic system.

Ultra-depleted Melts and the Formation of FAB

Melts crossing the crust/mantle boundary are thought to have a long history of melt-rock interaction over the course of their extraction from the asthenosphere (Kelemen et al., 1997; Korenaga and Kelemen, 1998). In this set of samples we see evidence for the interaction between melts with varying affinities and petrogenetic histories in the mantle transition zone (MTZ) of the Bonin Ridge. Pervasive transport of melt through the MTZ is suggested by the general lack of clinopyroxene and plagioclase in dunite and abundant clinopyroxene (with minor orthopyroxene) and plagioclase in wehrlite (Marchesi et al., 2009).

The presence of small or absent Eu anomalies in the REE patterns of the D31 clinopyroxene in samples with little or no plagioclase suggests that clinopyroxene was crystallizing before plagioclase by the migrating melt in an open system (Koga et al., 2001; Marchesi et al., 2009). Suppression of plagioclase and crystallization of clinopyroxene is generally attributed to the presence of low concentrations of water in a melt (Feig et al., 2006; and references therein).

A primitive parental magma composition is suggested by the high Cr_2O_3 and Mg# in the D31 pyroxene. Pyroxenes with high Mg#s are believed by some to crystallize by primitive MORB at moderately high pressures (i.e. >0.2 GPa) (Ross and Elthon, 1997). However, such pyroxenes are expected to have relatively high Al_2O_3 of up to 3% and 6% for orthopyroxene and clinopyroxene respectively (Seyler et al., 2001; Nonnotte et al., 2005, Marchesi et al., 2009). As is illustrated in Figures 5 and 6, the D31 pyroxenes do not follow this expected trend. This suggests a non-primitive MORB origin for these clinopyroxenes. However, the Cr# and TiO_2 contents of spinels associated with these clinopyroxenes have values in equilibrium with MORB similar to those of melt-rock reacted and depleted peridotites from mid-ocean ridges (Dick and

Bullen, 1984; Dick, 1989). These seemingly contradictory mineral compositions suggest that these phases did not crystallize from a single migrating aggregate MORB.

The high Mg#-Cr₂O₃ and low TiO₂ compositions of the clinopyroxenes suggest a primitive parental melt. The lack of orthopyroxene and abundance of clinopyroxene suggests the presence of water in the upper portions of the MTZ (probably at P ~0.2 GPa, Collot et al., 1987). Such conditions would favor crystallization of clinopyroxene at the expense of orthopyroxene (Feig et al. 2006). This is considered unusual in ocean ridge melts and characteristic of andesitic-boninitic sequences from convergent margins (Kelemen et al., 2003; Suhr et al., 2003; Marchesi et al., 2009). In contrast to the MORB dominated chemistry of melts at mid-ocean ridges, the association of arc tholeiites and variably depleted boninitic volcanic rocks is common in ophiolite sections with forearc affinities (Bedard et al., 1998; Kvassnes et al., 2004; Garrido et al., 2006).

Figure 9 shows chondrite-normalized (McDonough and Sun, 1995) trace element patterns for D31 clinopyroxenes. The trace element compositions of clinopyroxenes can be used to obtain information regarding the characteristic chemical signature of migrating liquids. This is calculated by inverting the trace element concentrations based on clinopyroxene/melt partition coefficients determined experimentally or from natural samples (Irving and Frey, 1984 and references therein; Bedard, 1994; Kelemen et al., 1997; Koga et al., 2001). Overall, the incompatible trace elements (i.e. HFSEs and LREEs) of the D31 clinopyroxenes are lower than those in gabbroic and wehrlitic rocks from the Oman MTZ that are interpreted to have crystallized from a MORB-like melt (Kelemen et al., 1997; Koga et al., 2001). They do however, overlap in part with samples from the Kohistan MTZ and the Massif du Sud ophiolite which are posited to be in equilibrium with boninitic melts (Dhuime et al., 2007; Garrido et al., 2007;

Marchesi et al., 2009).

This indicates that these samples are recording the migration and ascension of separate melt batches through the MTZ. For example, clinopyroxenes with lower La/Sm_N may be derived from a more depleted source or higher degree partial melts. Higher degree partial melts such as boninites would generally be depleted in oxides such as TiO₂ and CaO and relatively enriched in oxides like MgO and SiO₂. These higher degree partial melts are hard to create and are thought to be the result of addition of water to a peridotite source (Kushiro, 1975). This is consistent with the preferential crystallization of clinopyroxene before plagioclase inferred from the trace elements of D31 clinopyroxenes. This possible SiO₂-rich parental melt origin of the D31 clinopyroxenes is consistent with high degree partial melts derived from a high flux of aqueous fluids (Kushiro, 1975; Marchesi et al., 2009). However, this would cause saturation of orthopyroxene in the magma, and though it is rarely present, save for minor amounts, there is a characteristic lack of orthopyroxene in the Group M rocks.

It is possible that the D31 gabbroic and wehrlitic pyroxenes are derived from ascending single depleted MORB melt fractions in the mantle. These single fraction melts are indicated by the presence of highly depleted, orthopyroxene-saturated melts in the mantle sections of 'ocean ridge' ophiolites (e.g. Rampone et al., 1997; Dijkstra et al., 2003; Borghini et al., 2007). These cumulate pods are suggested to crystallize from the last melt increments produced by adiabatic upwelling of a MORB source (Dick, 1977). These melts tend to be highly reactive in the presence of lithospheric mantle (Rampone et al., 1997). Due to this reactivity, they are generally thought to be easily re-incorporated into the upper mantle and/or aggregated into more enriched melt fractions. This would owe to their rarely documented occurrence in the MTZ and lower oceanic crust (Ross and Elthon, 1993; Suhr et al., 1998; Coogan et al., 2000; Dick et al., 2010).

Marchesi et al. (2009) found similar evidence for a highly depleted melt in samples from the Massif du Sud ophiolite, to which they argue that it is unlikely that this type of highly depleted melt is derived from MORB-like melt fractions based on the ophiolites forearc environment of origin. This would make the melts more akin to the boninitic dunites and pyroxenites of the Bay of Islands ophiolite (Varfalvy et al., 1996; Suhr et al., 2003) and those which crystallized from re-melted, depleted, lithosphere which intrudes as depleted dykes in the Oman mantle section (Benoit et al., 1996; Kelemen et al., 1997a; Benoit et al., 1999; Python and Ceuleneer, 2003). This origin would be consistent with the D31 wehrlites and gabbros if they did not contain MORB-reacted spinels, which would be easily affected by interaction with a boninitic melt.

Figure 11 compares trace element compositions of modeled melts in equilibrium with D31 clinopyroxenes against FAB compositions from Ishizuka et al. (2011). The linear nature of the FAB array and the plotting of the modeled melts at the most depleted end of the array suggests a possible mixing line between an unknown enriched melt (Zr ~100 ppm) and a highly depleted end member represented by the D31 clinopyroxenes. The unknown enriched end member would be too enriched for an average MORB melt composition and thus may itself be a result of mixing. In fact, 5 to 7% fractional melting of a DMM source (Workman & Hart, 2005) refertilized by the addition of ~12% N-MORB (Sun and McDonough, 1989) would create a viable enriched end member in the FAB mixing array, with outliers falling along the fractional melting curve at higher melt fractions. However, this fractional melting model of a refertilized DMM source would lead to highly depleted melts at high melt fractions (i.e. $F > 15\%$) that are even more depleted than the modeled melts for the D31 clinopyroxenes. These modeled melts do plot relatively close to the composition of DMM, and thus may be a result of re-melting of

previously depleted DMM. This would suggest then that refertilization, although widespread enough to create an enriched source for a significant volume of melt, was localized and left large portions of previously depleted mantle undisturbed.

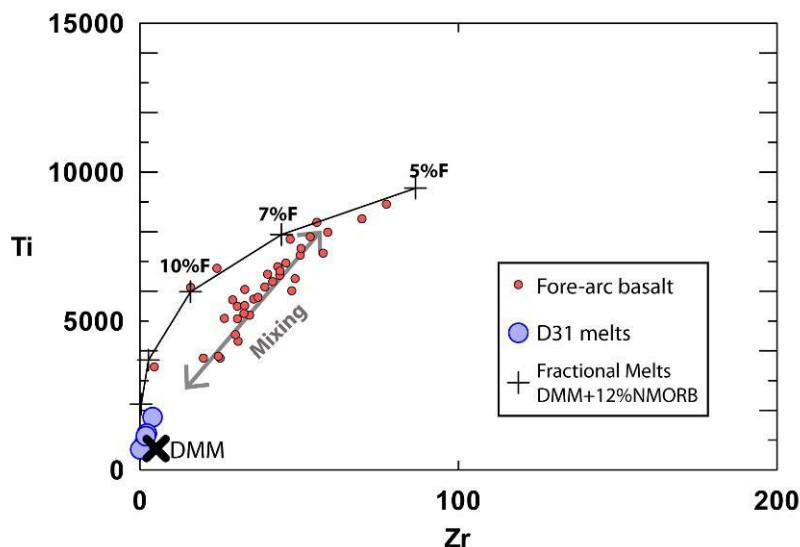


Figure 11: Zr vs Ti of FABs (Ishizuka et al., 2011) and equilibrium melts calculated for D31 clinopyroxenes. DMM is the data point from Workman and Hart (2005). The fractional melting curve plotted uses a source composition of DMM + 12% N-MORB (Sun and McDonough, 1989) which between 5 and 7% fractional melting replicates a possible enriched end-member for the FAB-D31 cpx mixing array.

The generally accepted model for subduction initiation in the IBM arc suggests that once the top of the down-going plate has passed beneath the base of the overriding lithosphere, asthenosphere from beneath both plates would naturally rush to fill the newly created void or ‘proto-mantle wedge’ (Stern & Bloomer, 1992; Stern, 2004). Melts from this upwelling asthenospheric mantle would, in effect, refertilize the previously depleted DMM present between the two plates (Fig. 12). This could create a mantle composition consistent with the proposed

model for the source of the enriched end member in the FAB mixing array. Further, evidence for the presence of ancient depleted mantle domains in the IBM forearc was reported by Parkinson et al. (1998) based on Re-Os isotopic analyses of forearc peridotites. Similar depleted mantle domains would likely be candidates for the source of the highly depleted end member that is evidenced by the D31 clinopyroxenes. It is thus likely that the rocks sampled by dredge D31 represent, in part, a zone where various melt fractions were mixing to create aggregated FAB melts. This would also suggest that the gradual transition from more enriched FABs to true boninites as the arc matured may not just represent the increasing amount of slab influence on melting, but also the gradual depletion of the initially refertilized source.

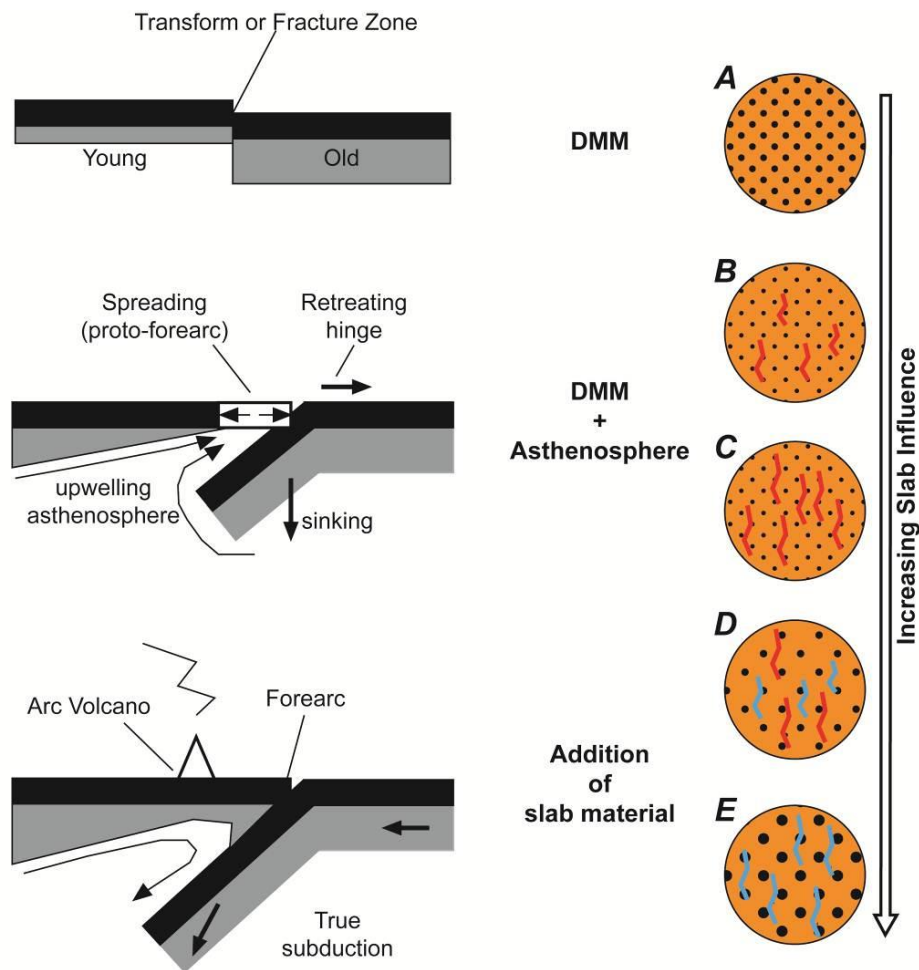


Figure 12: A schematic model for melting during subduction initiation. The left panel is from Stern (2004). Prior to initiation (A), the mantle has a DMM composition from a previous MOR melt extraction event. (B) As the older plate begins to sink and passes beneath the younger plate, upwelling asthenosphere rushes to fill the newly created void. This effectively refertilizes the mantle between the two plates. (C) As forearc spreading begins, both the DMM and refertilized mantle melts beneath the spreading center. (D) Once the subducting slab reaches a particular depth, it begins to contribute fluids and material to the mantle wedge and the forearc. Soon after this, spreading ceases in the forearc. (E) Once true subduction has begun, the volcanic arc moves landward and the melts are dominantly slab influenced.

CONCLUSIONS

The peridotites, wehrlites, and gabbros of KH07-02 dredge D31 represent a fossil mantle transition zone that was dominantly active during the initial stages of magmatism associated with subduction initiation of the IBM arc system. The various D31 lithologies are consistent with an origin through melt stagnation and subsequent melt-rock interaction within and along the periphery of melt conduits in the lower crust or crust/mantle transition similar to such sections in ophiolites and along MOR's.

Although alteration is present and variable, spinel is present in every rock type recovered by D31 and a dunite from D42 that is interpreted to be from the upper-lower crust. Major element analysis of spinels suggests the presence of two distinct groups of rocks based on composition, Group M and Group B. Group M spinels exhibit compositions consistent with spinels that have reacted with MORB-like melt and are lithologically limited to plagioclase-bearing peridotites, wehrlites, and primitive gabbroic rocks. Group B spinels are limited to dunites and pyroxene-poor harzburgites, and show a trend towards higher Cr#s and Mg#s away from that of Group M rocks, which is consistent with spinels that have reacted with boninite-like melts. The previously established age gap between the MORB-like FABs (50-52 Ma) and boninites (44-48 Ma) along the Bonin Ridge, combined with the lithologic constraints for the spinel groupings suggests that MORB melt-reaction occurred prior to boninite melt-reaction, and the dredge D31 rocks record a similar petrogenetic history as the volcanic rocks reported by Ishizuka et al. (2011). This suggests that a majority of the lower crust was created by forearc extension during/following subduction initiation and that later mature arc volcanism contributed little or no material to the lower crust save for dunite conduits.

Major and trace element compositions of clinopyroxenes in the D31 gabbros and

wehrlites fall in the range of some of the most depleted clinopyroxenes analyzed in abyssal and ophiolitic rocks. In particular, their trace element compositions are consistent with rocks of the Massif du Sud ophiolite (New Caledonia) (Marchesi et al., 2009) and the Kohistan mantle transition zone (Garrido et al., 2007) that are interpreted to have crystallized from boninitic melts. A boninitic origin is ruled out, however, on the basis that spinels in close association with the clinopyroxenes have MORB-reaction chemistries and show little or no evidence for reaction or equilibration with a boninitic melt. Further, geochemical modeling of melts in equilibrium with the clinopyroxenes suggests that they crystallized from a highly depleted, DMM-like melt which plots nicely as a depleted mixing end-member for FABs. This suggests that these clinopyroxenes crystallized from single, highly depleted melt fractions that had yet to aggregate into FAB. These single melt fractions are rarely documented due to their highly reactive nature and tendency to form cumulate pods or re-assimilate into the mantle.

An enriched end-member component for FAB mixing relative to the depleted end-member represented by the clinopyroxenes is modeled in accordance with models for subduction initiation and arc evolution. A mixture of DMM (Workman and Hart, 2005) with ~12% N-MORB (Sun and McDonough, 1989) best simulates the source of the enriched end-member, which would have been the result of refertilization of previously depleted mantle by material from the asthenosphere flowing in to fill the space created between the top of the down-going plate and the base of the over-riding plate. Melts created by 5-7% fractional melting of this DMM + 12% N-MORB source are the most likely end-member of the FAB mixing array, with outliers of the FAB array plotting exactly along the DMM+12% N-MORB fractional melting curve and the depleted end-member clinopyroxene parent melts falling to more enriched, almost DMM compositions. The presence of a highly depleted end-member is consistent with the

identification of preserved ancient depleted mantle domains in the IBM forearc by Parkinson et al. (1998).

This investigation of dredges D31 and D42 has provided an unusual glimpse into the inner workings of the lower arc crust. To date no in-situ lower arc crust has been sampled by drilling, although drilling of the seafloor around D42 is scheduled for 2014 by the Joides Resolution. This study provides an important complement to this proposed drilling leg in that it provides a preview of the types of rocks and the processes that are to be expected. The petrogenetic connection between these lower crustal rocks and the FABs recovered nearby suggests that the foundations of subduction zone arcs is created dominantly by MOR-like extension during subduction initiation and not during flux melting of the mature arc.

The IBM forearc, in particular the Bonin Ridge, represents an ‘ophiolite-in-waiting’. In fact, the stratigraphy of the Bonin Ridge and the geochemical and lithological characteristics of the rocks from dredge D31 indicate that the IBM forearc is very similar to well characterized ophiolite sections around the world. Stern (2004) extrapolates from both previous and similar observations and the IBM forearc’s tectonic setting, which favors the obduction of ophiolites, that SSZ ophiolites are packages or pieces of forearc material that formed during SNSZ events that are later emplaced as the result of collision events. If this is the case, then 10,000 kilometers or more of the western Pacific could be lined with ophiolites-in-waiting. This suggests that ophiolites are not unique in the geologic record and are thus an inevitable consequence of plate tectonics.

REFERENCES

- Ampferer, O., 1906. Über das Bewegungsbild von Faltengebirgen. *Jahrb. Geol. Reichsanstalt*, 56:539-622.
- Amstutz, A., 1951. Sur l'évolution des structures alpines. *Archives Sci.*, 4:323-329.
- Arai, S., 1992. Chemistry of chromian spinel in volcanic rocks as a potential guide to magma chemistry. *Mineralogy Magazine*, 56:173-184.
- Arai, S., 1994. Characterization of spinel peridotites by olivine-spinel compositional relationships: review and interpretation. *Chemical Geology*, 113:191-204.
- Arai, S. & Matsukage, K., 1996. Petrology of gabbro-troctolite-peridotite complex from Hess Deep, equatorial Pacific: implications for mantle-melt interaction within the oceanic lithosphere. In: Mevel, C., Gillis, K. M., Allan, J. F. & Meyer, P. S. (eds) *Proceedings of the Ocean Drilling Program*, 147. College Station, TX: Ocean Drilling Program, pp. 135-155.
- Bedard, J.H., 1994. A procedure for calculating the equilibrium distribution of trace elements among the minerals of cumulate rocks, and the concentration of trace elements in the coexisting liquids. *Chemical Geology*, 118: 143-153.
- Bedard, J.H., Lauziere, K., Tremblay, A., Sangster, A., 1998. Evidence for forearc seafloor spreading from the Betts Cove ophiolite, Newfoundland: oceanic crust of boninitic affinity. *Tectonics*, 284: 233-245.
- Bedard, J. H., Hebert, R., Berclaz, A. & Varfalvy, V., 2000. Syntaxis and the genesis of lower oceanic crust. In: Dilek, Y., Moores, E.M., Elthon, D. & Nicolas, A. (eds) *Ophiolites and Oceanic Crust: New Insights from Field Studies and the Ocean Drilling Program*. Geological Society of America, Special Papers 349, 349, pp. 105-119.

- Benoit, M., Ceuleneer, G., Polvé, M., 1999. The remelting of hydrothermally altered peridotite at mid-ocean ridges by intruding mantle diapirs. *Nature*, 402:514–518.
- Benoit, M., Polvé, M., Ceuleneer, G., 1996. Trace element and isotopic characterization of mafic cumulates in a fossil mantle diapir (Oman ophiolite). *Chemical Geology*, 134:199–214.
- Bloomer, S.H., 1983. Distribution and origin of igneous rocks from the landward slopes of the Mariana Trench: implications for its structure and evolution. *Journal of Geophysical Researches*, 88:7411–7428.
- Bloomer, S.H., Taylor, B., MacLeod C.J. et al., 1995. Early arc volcanism and ophiolite problem: A perspective from drilling in the Western Pacific. In: Taylor B. & Natland J. (eds). *Active Margins and Marginal Basins of the Western Pacific*. Geophysical Monograph, 88: 1–30. American Geophysical Union, Washington, DC.
- Bonatti, E., Peyve, A., Kepezhinskas, P., Kurentsova, N., Seyler, M., Skolotnev, S. & Udintsev, G., 1992. Upper mantle heterogeneity below the Mid-Atlantic Ridge, 08°15'N. *Journal of Geophysical Researches*, 97:4461–4476.
- Borghini, G., Rampone, E., Crispini, L., De Ferrari, R., Godard, M., 2007. Origin and emplacement of ultramafic–mafic intrusions in the Erro-Tobbio mantle peridotite (Ligurian Alps, Italy). *Lithos*, 94:210–229.
- Boudier, F., Coleman, R.G., 1981. Cross section through the peridotite in the Samail Ophiolite, southeastern Oman Mountains. *Journal of Geophysical Researches*, 86:2573–2592.
- Boudier, F. & Nicolas, A., 1995. The nature of the Moho transition zone in the Oman ophiolite. *Journal of Petrology*, 36:777–796.
- Brunelli, D. & Seyler, M., 2010. Asthenospheric percolation of alkaline melts beneath the St. Paul region (Central Atlantic Ocean). *Earth and Planetary Science Letters*, 289:393–405.

- Cann, J.R., 1970. Petrology of basalts dredged from the Gulf of Aden. *Deep-Sea Research* 17:477.
- Ceuleneer, G., Nicolas, A., 1985. Structures in podiform chromite from the Maqsad district (Sumail ophiolite, Oman). *Mineral Deposita*, 20:177-185.
- Choi, S.H., Shervais, J.W., Mukasa, S.B., 2008. Supra-subduction and abyssal mantle peridotites of the Coast Range ophiolite, California. *Contributions to Mineralogy and Petrology*, 156:551–576.
- Collot, J.-Y., Malahoff, A., Récy, J., Latham, G., Missègue, F., 1987. Overthrust emplacement of New Caledonia ophiolite: geophysical evidence. *Tectonics*, 6:215–232.
- Coogan, L.A., Kempton, P.D., Saunders, A.D., Norry, M.J., 2000. Melt aggregation within the crust beneath the Mid-Atlantic Ridge: evidence from plagioclase and clinopyroxene major and trace element compositions. *Earth Planetary Science Letters*, 176:245–257.
- Danyushevsky, L.V., Sobolev, A.V., and Falloon, T.J., 1995. North Tongan high-Ca boninite petrogenesis- The role of Samoan plume and subduction zone-transform fault transition. *Journal of Geodynamics*, 20:219-241.
- DeBari, S.M., Taylor, B., Spencer, K., Fujioka, K., 1999. A trapped Philippine Sea plate origin for MORB from the inner slope of the Izu-Bonin trench, *Earth and Planetary Science Letters*, 174:183–197.
- Dewey, J.F., Casey, J.F., 2011. The origin of obducted large-slab ophiolite complexes. In Brown, D., Ryan, P.D., et al., 2011. In: *Arc-Continent Collision*, Springer Berlin Heidelberg: 431-444.
- Dhuime, B., Bosch, D., Bodinier, J.L., Garrido, C.J., Bruguier, O., Hussain, S.S., and Dawood, H., 2007. Multistage evolution of the Jijal ultramafic-mafic complex (Kohistan, N.

- Pakistan): Implications for building the roots of island arcs. *Earth and Planetary Science Letters*, 261:179-200.
- Dick, H. J. B., 1977. Evidence of partial melting in the Josephine Peridotite. In: Dick, H. J. B. (ed.) *Magma Genesis*. Portland, OR: Oregon Department of Geology and Mineral Industries, pp. 59-62.
- Dick, H.J.B., 1989. Abyssal peridotites, very slow spreading ridges and ocean ridge magmatism. In: Saunders, A.D., Norry, M.J. (Eds.), *Magmatism in the Ocean Basins: Geological Society, London, Special Publications*, 42:71–105.
- Dick, H.J.B., Bullen, T., 1984. Chromian spinel as a petrogenetic indicator in abyssal and Alpine-type peridotites and spatially associated lavas. *Contributions to Mineralogy and Petrology*, 86:54–76.
- Dick, H.J.B., Natland, J.H., 1996. Late stage melt evolution and transport in the shallow mantle beneath the East Pacific Rise. *ODP Scientific Results*, 147:103-134.
- Dick, H.J.B., Lisseberg, C.J., Warren, J.M., 2010. Mantle melting, melt transport, and delivery beneath a slow-spreading ridge: The paleo-MAR from 23°15'N to 23°45'N, *Journal of Petrology*, 51:425-467.
- Dijkstra, A.H., Barth, M.G., Drury, M.R., Mason, P.R.D., Vissers, R.L.M., 2003. Diffuse porous melt flow and melt–rock reaction in the mantle lithosphere at a slow-spreading ridge: a structural petrology and LA-ICP-MS study of the Othris Peridotite Massif (Greece). *Geochemistry Geophysics Geosystems*, 4:8613. doi:8610.1029/2001GC000278.
- Drouin, M., Godard, M. & Ildefonse, B., 2007. Origin of olivine-rich troctolites from IODP Hole U1209D in the Atlantis Massif (Mid-Atlantic Ridge): Petrostructural and geochemical study. *EOS Transactions American Geophysical Union* 88(52), Abstract T53B-1300.

- Drouin, M., Godard, M., Ildefonse, B., Bruguier, O., Garrido, C. J., 2009. Geochemical and petrographic evidence for magmatic impregnation in the oceanic lithosphere at Atlantis Massif, Mid-Atlantic Ridge (IODP Hole U1309D, 308N). *Chemical Geology*, 264:71-88.
- Drouin, M., Ildefonse, B. & Godard, M., 2010. A microstructural imprint of melt impregnation in slow-spread lithosphere: olivine-rich troctolites from the Atlantis Massif (Mid-Atlantic Ridge 308N, IODP Hole U1309D). *Geochemistry, Geophysics, Geosystems*, 11:Q06003, doi:10.1029/2009GC002995.
- Elthon, D., Casey, J. F. & Komor, S., 1982. Mineral chemistry of ultramafic cumulates from the North Arm Mountain Massif of the Bay of Islands ophiolite: evidence for high pressure crystal fractionation of oceanic basalts. *Journal of Geophysical Researches*, 87:8717-8734.
- Feig, S.T., Koepke, J., and Snow, J.E., 2006. Effect of water on tholeiitic basalt phase equilibria: an experimental study under oxidizing conditions. *Contributions to Mineralogy and Petrology*, 152:611-638.
- Fryer, P., Pearce, J. A., Stokking, L. B., et al., 1992. *Proceedings of the Ocean Drilling Program, Scientific Results*, 125.
- Garrido, C.J., Bodinier, J.L., Burg, J.P., Zeilinger, G., Hussain, S.S., Dawood, H., Chaudhry, M.N., Gervilla, F., 2006. Petrogenesis of mafic garnet granulite in the lower crust of the Kohistan paleo-arc complex (Northern Pakistan): implications for intra-crustal differentiation of island arcs and generation of continental crust. *Journal of Petrology*, 47:1873–1914.
- Garrido, C.J., Bodinier, J.-L., Dhuime, B., Bosch, D., Chanefo, I., Bruguier, O., Hussain, S.S., Dawood, H., Burg, J.-P., 2007. Origin of the island arc Moho transition zone via melt–

- rock reaction and its implications for intracrustal differentiation of island arcs: evidence from the Jijal complex (Kohistan complex, northern Pakistan). *Geology*, 35:683–686.
- Godard, M., Lagabrielle, Y., Alard, O., Harvey, J., 2008. Geochemistry of the highly depleted peridotites drilled at ODP Sites 1272 and 1274 (Fifteen-Twenty Fracture Zone, Mid-Atlantic Ridge): implications for mantle dynamics beneath a slow spreading ridge. *Earth Planetary Science Letters*, 267:410–425.
- Godard, M., Awaji, S. & Hansen, H., 2009. Geochemistry of a long in-situ section of intrusive slow-spread oceanic lithosphere: Results from IODP Site U1309 (Atlantis Massif, 308N Mid-Atlantic Ridge). *Earth and Planetary Science Letters*, 279:110-122.
- Grove, T. L., Kinzler, R. J. & Bryan, W.B., 1990. Natural and experimental phase relations of lavas from Serocki volcano. In: Detrick, R., Honnorez, J., Bryan, W. B. & Juteau, T. et al. (eds) *Proceedings of the Ocean Drilling Program, Scientific Results*, 106/109. College Station TX: Ocean Drilling Program, pp. 9-17.
- Grove, T. L., Kinzler, R. J. & Bryan, W. B., 1992. Fractionation of mid-ocean ridge basalt. In: Morgan, J. P., Blackman, D. K. & Sinton, J. M. (eds) *Mantle Flow and Melt Generation at Mid-Ocean 70 Ridges*. *Geophysical Monograph, American Geophysical Union* 71, 71, pp. 281-311.
- Gurnis, M., Hall, C., Lavier, L., 2004. Evolving force balance during incipient subduction. *Geochemistry Geophysics Geosystems* 5. DOI:10.1029/2003GC000681.
- Hall, C.E., Gurnis, M., Sdrolias, M., Lavier, L.L., Muellar, R.D., 2003. Catastrophic initiation of subduction following forced convergence across fracture zones. *Earth and Planetary Science Letters*, 212:15–30.
- Harigane, Y., Michibayashi, K., Morishita, T., Tani, K., Dick, H.J.B., Ishizuka, O., In

- Preparation. The earliest mantle fabrics formed during subduction zone infancy.
Submitted to Earth and Planetary Science Letters.
- Hart, S. R. & Dunn, T., 1993. Experimental cpx/melt partitioning of 24 trace elements.
Contributions to Mineralogy and Petrology, 113:18.
- Hellebrand, E., Snow, J.E., Dick, H.J.B., Hofmann, A.W., 2001. Coupled major and trace elements as indicators of the extent of melting in mid-ocean-ridge peridotites. *Nature* 410:677–681
- Hellebrand, E., Snow, J.E., Dick, H.J.B., Hofmann, A.W., 2002. Garnet-field melting and later-stage refertilization in ‘residual’ abyssal peridotites from the central Indian Ridge. *Journal of Petrology*, 43:2305–2338.
- Hussong, D.M., Uyeda, S., et al., 1981. Initial Reports of the Deep Sea Drilling Project, Leg 60, 60. U.S. Government Printing Office, Washington D.C.. 929 pp.
- Irving, A.J., Frey, F.A., 1984. Trace element abundances in megacrysts and their host basalts: Constraints on partition coefficients and megacrysts genesis. *Geochimica et Cosmochimica Acta*, 48: 1201-1221.
- Ishizuka, O, Tani, K, Reagan, MK, Kanayama, K, Umino, S, Harigane, Y, Sakamoto, I, Miyajima, Y, Yuasa, M, Dunkley, D.J., 2011. The timescales of subduction initiation and subsequent evolution of an oceanic island arc. *Earth and Planetary Science Letters*, 306:229–240.
- Ishii, T., Robinson, P.T., Maekawa, H., Fiske, R., 1992. Petrological studies of peridotites from diapiric serpentinite seamounts in the Izu-Ogasawara-Mariana forearc, Leg 125. *Proceedings of the Ocean Drilling Program Scientific Results*, 125: 445-485.

- Johnson, K.T.M., Dick, H.J.B., Shimizu, N., 1990. Melting in the oceanic upper mantle: an ion microprobe study of diopsides in abyssal peridotites. *Journal of Geophysical Research* 95:2661–2678.
- Kamenetsky, V.S., Sobolev, A.V., Eggins, S.M., Crawford, A.J., Arculus, R.J., 2002. Olivine enriched melt inclusions in chromites from low-Ca boninites, Cape Vogel, Papua NewGuinea: evidence for ultramafic primary magma, refractory mantle source and enriched components. *Chemical Geology*, 183:287–303.
- Karig, D. E., Anderson, R. N., Bibee, L. D., 1978. Characteristics of back-arc spreading in the Mariana Trough. *Journal of Geophysical Research*, 83:1213-1226.
- Kelemen, P.B., Dick, H.J.B., 1995. Focused melt flow and localized deformation in the upper mantle: Juxtaposition of replacive dunite and ductile shear zones in the Josephine peridotite, SW Oregon. *Journal of Geophysical Research*, 100: 423-438.
- Kelemen, P.B., Dick, H.J.B., Quick, J.E., 1992. Formation of harzburgite by pervasive melt/ rock reaction in the upper mantle. *Nature*, 358:635–641.
- Kelemen, P.B., Hanghøj, K., Greene, A.R., 2003. In: Rudnick, R. (Ed.), One view of the geochemistry of subduction-related magmatic arcs, with an emphasis on primitive andesite and lower crust. In: *The Crust, Treatise on Geochemistry*, vol. 3. Elsevier, pp. 593–659.
- Kelemen, P.B., Koga, K., Shimizu, N., 1997. Geochemistry of gabbro sills in the crust-mantle transition zone of the Oman ophiolite: implications for the origin of the oceanic lower crust. *Earth and Planetary Science Letters*, 146:475-488.
- Kelemen, P.B., Shimizu, N., Salters, V.J.M., 1995. Extraction of mid-ocean-ridge basalt from the upwelling mantle by focused flow of melt in dunite channels. *Nature*, 375:747–753.

- Kelemen, P. B., Kikawa, E. & Miller, D. J. et al. (eds), 2004. Proceedings of the Ocean Drilling Program, Part A: Initial Reports, 209. College Station, TX: Ocean Drilling Program.
- Kobayashi, K., Nakada, M., 1979. Magnetic anomalies and tectonic evolution of the Shikoku inter-arc basin. In Uyeda, S., et al. (Eds.), *Advances in Earth and Planetary Sciences*, 6:391-402.
- Kodaira, S., Noguchi, N., Takahashi, N., Ishizuka, O., Kaneda, Y., 2010. Evolution from fore-arc oceanic crust to island arc crust: a seismic study along the Izu–Bonin forearc. *Journal of Geophysical Research*, 115:B09102.
- Koga, K.T., Kelemen, P.B., Shimizu, N., 2001. Petrogenesis of the crust–mantle transition zone and the origin of lower crustal wehrlite in the Oman ophiolite. *Geochemistry Geophysics Geosystems*, 2. 2000GC000132.
- Korenaga, J., Kelemen, P.B., 1998. Melt migration through the oceanic lower crust: a constraint from melt percolation modeling with finite solid diffusion. *Earth and Planetary Science Letters*, 156:1-11.
- Kushiro, I., 1975. On the nature of silicate melt and its significance in magma genesis: regularities in the shift of the liquidus boundaries involving olivine, pyroxene, and silica minerals. *American Journal of Science*, 275:411–431.
- Kvassnes, A.J.S., Hetland Strand, A., Moen-Eikeland, H., Birger Pedersen, R., 2004. The Lyngen Gabbro: the lower crust of an Ordovician incipient arc. *Contributions to Mineralogy & Petrology*, 148:358–379.
- Kvassnes, A. J. S. & Grove, T., 2008. How partial melts of mafic lower crust affect ascending magmas at oceanic ridges. *Contributions to Mineralogy and Petrology*, 156:49-71.
- Lissenberg, C.J., Dick, H.J.B., 2008. Melt-rock reaction in the lower oceanic crust and its

- implications for the genesis of mid-ocean ridge basalt. *Earth and Planetary Science Letters*, 271:311-325.
- Lissenberg, C.J., MacLeod, C.J., Howard, K.A., Godard, M., In Press. Pervasive reactive melt migration through fast-spreading lower oceanic crust (Hess Deep, equatorial Pacific Ocean). *Earth and Planetary Science Letters* (2012).
<http://dx.doi.org/10.1016/j.epsl.2012.11.012>
- MacLeod, C.J., Yaouancq, G., 2000. A fossil melt lens in the Oman ophiolite: Implications for magma chamber processes at fast spreading ridges. *Earth and Planetary Science Letters*, 176:357-373.
- Maehara, K. and Maeda, J., 2004. Evidence for high-Ca boninite magmatism from Paleogene primitive low-K tholeiite, Mukoojima, Hahajime Island group, southern Bonin (Ogasawara) forearc, Japan. *Island Arc* 13:452-465.
- Marchesi, C., Garrido, C.J., Godard, M., Belley, F., Ferre, E., 2009. Migration and accumulation of ultra-depleted subduction-related melts in the Massif du Sud ophiolite (New Caledonia). *Chemical Geology*, 266: 171-186.
- McDonough, W.F., Sun, S.-S., 1995. The composition of the Earth. *Chemical Geology*, 120:223–253.
- Medaris, L.G., 1972. High-pressure peridotites in southwestern Oregon. *Geological Society of America Bulletin*, 83:41.
- Meijer, A., 1980. Primitive arc volcanism and a boninite series: examples from western Pacific island arcs. In: Hayes, D.E. (Ed.), *The Tectonic Evolution of Southeast Asian Seas and Islands*. :Amer. Geophys. Union Monogr., 23.AGU, Washington, D.C., pp. 269–282.

- Meyer, P. S., Dick, H. J. B. & Thompson, G., 1989. Cumulate gabbros from the Southwest Indian Ridge, 548S, 7816'E: implications for magmatic processes at a slow spreading ridge. *Contributions to Mineralogy and Petrology*, 103:44-63.
- Moore, E.M. and Vine, F.J., 1971. Troodos Massif, Cyprus and other ophiolites as oceanic crust: Evaluation and implications. *Philosophical Transactions of the Royal Society of London Series A-Mathematical and Physical Sciences*, 268:443.
- Morishita, T., Tani, K., Shukono, H., Harigane, Y., Tamura, A., Kumagai, H., and Hellebrand, E., 2011. Diversity of melt conduits in the Izu-Bonin-Mariana forearc mantle: Implications for the earliest stage of arc magmatism: *Geology*, 39:411–414.
doi:10.1130/G31706.1.
- Natland, J.H., Dick, H.J.B., 1996. Melt migration through high-level gabbroic cumulates of the East Pacific Rise at Hess Deep: the origin of magma lenses and the deep crustal structure of fast spreading ridges. In: Mevel, C., Gillis, K.M., Allan, J.F., Meyer, P.S. (Eds.), *Proceedings of the Ocean Drilling Program. Scientific Results*, vol. 147. Ocean Drilling Program, College Station TX, pp. 21–58.
- Nicolas, A., 1989. *Structures of Ophiolites and Dynamics of Oceanic Lithosphere*, 367 pp., Kluwer, Dordrecht.
- Nicolas, A., Violette, J.F., 1982. Mantle flow at oceanic spreading centers: models derived from ophiolites. *Tectonophysics*, 81:319-339.
- Nicolas, A. & Prinzhofer, A., 1983. Cumulative or residual origin for the transition zone in ophiolites: structural evidence. *Journal of Petrology*, 24:188-206.

- Nonnotte, P., Ceuleneer, G., Benoit, M., 2005. Genesis of andesitic–boninitic magmas at mid-ocean ridges by melting of hydrated peridotites: Geochemical evidence from DSDP Site 334 gabbro-norites. *Earth and Planetary Science Letters*, 236:632–653.
- Parkinson, I.J., Pearce, J.A., 1998. Peridotites from the Izu-Bonin-Mariana forearc (ODP Leg 125); evidence for mantle melting and melt-mantle interaction in a supra-subduction zone setting, *Journal of Petrology*, 39:1577– 1618.
- Parlak O, Delaloye M, Bi'ngo'l E (1996) Mineral chemistry of ultramafic and mafic cumulates as an indicator of the arc-related origin of the Mersin ophiolite (southern Turkey). *Geol Rundsch*, 85:647–661.
- Pearce, J.A. and Cann, J.R., 1973. Tectonic setting of basic volcanic rocks determined using trace element analyses. *Earth and Planetary Science Letters*, 19:290-300.
- Pearce, J.A., Thirlwall, M.F., Ingram, G., Murton, B.J., Arculus, R.J., van der Laan, S.R., 1992. Isotopic evidence for the origin of boninites and related rocks drilled in the Izu– Bonin (Ogasawara) fore-arc, Leg 125. *Proceedings of the Ocean Drilling Program Scientific Results*, 125:237–261.
- Pearce, J.A., Subduction zone ophiolites, In: Y. Dilek, S. Newcomb (Eds.), *Ophiolite Concept and the Evolution of Geological Thought*. Special Paper 373, Geological Society of America, Boulder, 2003, pp. 269– 294.
- Piccardo, G. B., Zanetti, A., Poggi, E., Spagnolo, G. & Muntener, O., 2006. Melt/peridotite interaction in the southern Lanzo peridotite: Field, textural and geochemical evidence. *Lithos*, 94:181-209.
- Presnall, D.C., Dixon, S.A., Dixon, J.R., O'Donnell, T.H., Brenner, N. L., Schrock, R. L. & Dycus, D.W., 1978. Liquidus phase relations on the join diopside¹forsterite¹anorthite from 1 atm

- to 20 kbar: their bearing on the generation and crystallization of basaltic magma. *Contributions to Mineralogy and Petrology*, 66:203-220.
- Python, M., Ceuleneer, G., 2003. Nature and distribution of dykes and related melt migration structures in the mantle section of the Oman ophiolite. *Geochemistry Geophysics Geosystems*, 4. doi:10.1029/2002GC000354.
- Quick, J. E., 1981. The origin and significance of large, tabular dunite bodies in the Trinity Peridotite, Northern California. *Contributions to Mineralogy and Petrology*, 78:413-422.
- Ramp, L., 1961. Chromite in southwestern Oregon. *Bulletin-Oregon Department of Geology and Mineral Industry*, 52:1-169.
- Rampone, E., Piccardo, G.B., Vannucci, R., Bottazzi, P., 1997. Chemistry and origin of trapped melts in ophiolitic peridotites. *Geochimica et Cosmochimica Acta*, 61:4557–4569.
- Ranero, C.R., Morgan, J.P., McIntosh, K., Refchert, C., 2003. Bending related faulting and mantle serpentinization at the Middle America trench. *Nature*, 425:367– 373.
- Ranero, C.R., Sallares, V., 2004. Geophysical evidence for hydration of the crust and mantle of the Nazca plate during bending at the north Chile trench. *Geology*, 32:549–552.
- Reagan, M.K., Meijer, A., 1984. Geology and geochemistry of early arc volcanic rocks from Guam. *Geological Society of America Bulletin*, 95:701–713.
- Renna, M. R. & Tribuzio, R., 2011. Olivine-rich troctolites from Ligurian ophiolites (Italy): evidence for impregnation of replacive 65 mantle conduits by MORB-type melts. *Journal of Petrology*, 52:1763-1790.
- Roeder, P. L. & Reynolds, I., 1991. Crystallization of chromite and chromium solubility in basaltic melts. *Journal of Petrology*, 32:909-934.

- Ross, K., Elthon, D., 1993. Cumulates from strongly depleted mid-ocean ridge basalt. *Nature*, 365:826–829.
- Ross, K., Elthon, D., 1997. Cumulus and postcumulus crystallization in the oceanic crust: major and trace element geochemistry of LEG 153 gabbroic rocks. In: Karson, J.A., Cannat, M., Miller, D.J., Elthon, D. (Eds.), *Proceedings of the Ocean Drilling Program, Scientific Results*, 153:333–350.
- Sanfilippo, A., 2011. The generation of lower oceanic crust in (ultra-) slow spreading settings: Insights from the Alpine ophiolites and from the Godzilla Megamullion (Parece Vela basin), PhD thesis, Università degli Studi di Pavia.
- Sanfilippo, A., Tribuzio, R., 2012. Building of the deepest crust at a 85 fossil slow-spreading centre (Pineto gabbroic sequence, Alpine Jurassic ophiolites). *Contributions to Mineralogy and Petrology*, doi:10.1007/s00410-012-0831-8.
- Sanfilippo, A., Dick, H.J.B., Ohara, Y., 2013. Melt-rock reaction in the mantle: Mantle troctolites from the Parece Vela Ancient back-arc spreading center. *Journal of Petrology*, doi:10.1093/petrology/egs089.
- Savel'yeva, G.N., Shcherbakov, S.A., Denisova, Y.A., 1980. The role of high temperature in the development of dunite bodies in harzburgites. *Geotectonics*, 11:175-182.
- Sdrolias, M., Roest, W.R., Muller, R. D., 2004. An expression of Philippine Sea plate rotation: the Parece Vela and Shikoku Basins: *Tectonophysics*, 394:69-86.
- Seyler, M., Toplis, M.J., Lorand, J.-P., Luguët, A., Cannat, M., 2001. Clinopyroxene microtextures reveal incompletely extracted melts in abyssal peridotites. *Geology*, 29:155–158.

- Shervais, J.W., 2001. Birth, death, and resurrection: the life cycle of suprasubduction zone ophiolites, *Geochemistry, Geophysics, Geosystems*, 2. (Paper 2000GC000080).
- Stern, R.J., Bloomer, S.H., 1992. Subduction zone infancy: examples from the Eocene Izu–Bonin–Mariana and Jurassic California Arcs. *Geological Society of America Bulletin*, 104:1621–1636.
- Stern, R.J., Smoot, N.C., 1998. A bathymetric overview of the Mariana forearc. *The Island Arc*, 7:525– 540.
- Stern, R.J., Fouch, M.J., Klemperer, S., An overview of the Izu-Bonin-Mariana subduction factory, In: J. Eiler (Ed.), *Inside the Subduction Factory*, vol. 138, American Geophysical Union, *Geophysical Monograph*, Washington DC, 2003, pp. 175– 222.
- Stern, R.J., 2004. Subduction initiation: spontaneous and induced. *Earth and Planetary Science Letters*, 226: 275-292.
- Suhr, G., Hellebrand, E., Snow, J.E., Seck, H.A., Hofmann, A.W., 2003. Significance of large, refractory dunite bodies in the upper mantle of the Bay of Islands Ophiolite. *Geochemistry Geophysics Geosystems*, 4:8605. doi:8610.1029/2001GC000277.
- Suhr, G., Seck, H.A., Shimizu, N., Gunther, D., Jenner, G., 1998. Infiltration of refractory melts into the lowermost oceanic crust: evidence from dunite- and gabbro-hosted clinopyroxenes in the Bay of Islands Ophiolite. *Contributions to Mineralogy and Petrology*, 131:136–154.
- Suhr, G., 2004. Small scale mantle heterogeneity as observed in a 10 M section of peridotite (Site 1274, ODP Leg 209): relation to melt-rock reaction. *International Geological Congress*, 32:506–507.
- Suhr, G., Hellebrand, E., Johnson, K., and Brunelli, D., 2008. Stacked gabbro units and

- intervening mantle: A detailed look at a section of IODP Leg 305, Hole U1309D: *Geochemistry Geophysics Geosystems*, 9. doi:10.1029/2008GC002012.
- Sun, S.-S., McDonough, W.F., 1989. Chemical and isotopic systematics of oceanic basalts: implications for mantle composition and processes. In: Saunders, A.D., Norry, M.J. (Eds.), *Magmatism in the Ocean Basins: Geological Society Special Publication*, 42:313–345.
- Tamura, A., Arai, S., Ishimaru, S. & Andal, E. S., 2008. Petrology and geochemistry of peridotites from IODP Site U1309 at Atlantis Massif, MAR 308N: micro- and macro-scale melt penetrations into peridotites. *Contributions to Mineralogy and Petrology*, 155:491-509.
- Tartarotti, P., Susini, S., Nimis, P. & Ottolini, L., 2002. Melt migration in the upper mantle along the Romanche Fracture Zone (Equatorial Atlantic). *Lithos*, 63:125-14.
- Tormey, D. R., Grove, T. L. & Bryan, W. B., 1987. Experimental petrology of normal MORB near the Kane Fracture Zone: 22°-25°N, Mid-Atlantic Ridge. *Contributions to Mineralogy and Petrology*, 96:121-139.
- Tribuzio, R., Tiepolo, M., Fiameni, S., 2008. A mafic-ultramafic cumulate sequence derived from boninites-type melts (Niagara Icefalls, northern Victoria Land, Antarctica). *Contributions to Mineralogy and Petrology*, 155:619-633.
- Umino, S., 1985. Volcanic geology of Chichijima, the Bonin Islands (Ogasawara Islands). *Journal of the Geological Society of Japan*, 91:505–523.
- Varfalvy, V., Hébert, R., Bédard, J.H., 1996. Interactions between melts and upper-mantle peridotites in the North Arm Mountain massif, Bay of Islands ophiolite, Newfoundland,

- Canada: implications for the genesis of boninitic and related magmas. *Chemical Geology*, 129:71–90.
- White, D.A., Roeder, D.H., Nelson, T.H., Crowell, J.C., 1970. Subduction. *Geological Society of America Bulletin*, 81:3431-3432.
- Workman, R.K., Hart, S.R., 2005. Major and trace element composition of the depleted MORB mantle (DMM). *Earth and Planetary Science Letters*, 231:53–72.
- Yang, H. J., Kinzler, R. J. & Grove, T. L., 1996. Experiments and models of anhydrous, basaltic olivine-plagioclase-augite saturated melts from 0.001 to 10 kbar. *Contributions to Mineralogy and Petrology*, 124:1-18.

Appendix 1: Analytical Methods and Procedures

Electron Microprobe Methods

All samples which had sufficient grains for analysis were analyzed for spinel, clinopyroxene, orthopyroxene, and olivine major and minor elements. Spinel analyses were performed on both the Cameca SX-100 electron microprobe at Texas A&M University in early summer of 2012 and the Cameca SX-50 electron microprobe at the University of Houston in late summer of 2012. Clinopyroxene, orthopyroxene, and olivine analyses were performed on the Cameca SX-50 electron microprobe at Texas A&M University in early summer 2012. The composition of all synthetic and natural standards used for analysis can be found in Table A1.1. Collected data was corrected for absorption, atomic number, and fluorescence (ZAF) by the software provided by Cameca. Analytical conditions for each phase can be found in Tables A1.2 – A1.6.

Table A1.1: EMP Standard Compositions

Standard	Si	Al	Fe	Mg	Ca	Na	K	Ti	P
<u>UH</u>									
Chromite23	-	0.0519	0.1002	0.0906	0.0008	-	-	-	-
Gahnite25	-	0.2993	0.0153	-	-	-	-	-	-
Ni Metal*	-	-	-	-	-	-	-	-	-
Rhodonite72	0.2196	-	0.0275	0.0034	0.0562	-	-	-	-
Ilmenite27	-	-	0.3596	0.0019	-	-	-	0.2723	-
<u>TAMU</u>									
3olivine	0.1821	-	0.1292	0.2682	-	-	-	-	-
3chromite	-	0.0525	0.1014	0.0917	0.0009	-	-	-	-
3ilmenite	-	-	0.3617	0.0019	-	-	-	0.2740	-
5diopside	0.2580	0.0023	0.0069	0.1082	0.1800	0.0028	-	0.0002	-
5spessart.	0.1685	0.1092	0.0129	-	0.0033	-	-	0.0002	-
5albite	0.3185	0.1046	0.0001	-	0.0027	0.0850	0.0019	-	-
5orthoclase	0.3029	0.0886	0.0140	-	-	0.0068	0.0129	-	-
7enstCF	0.2706	0.0098	0.0010	0.2414	0.0008	-	-	-	-
7ni*	-	-	-	-	-	-	-	-	-

Table A1.1: Composition of standards from the Texas A&M and University of Houston EMP labs. *synthetic stan

Spinel Analytical Conditions						Accelerating Potential: 15 kV
University of Houston			Spot Size: 1 μ m		Beam Current: 20 nA	
Standard	SP1 (LIF)	SP2 (TAP)	SP3 (PET)	SP4 (PET)	EDS	Backgrounds
Chromite23		Al (60)	Cr (30)		Mg (100), Fe(100)	Al: \pm 800; Cr: \pm 500
Diopside15					Si (100), Ca (100)	
Rutile81				Ti (40)		Ti: \pm 500
Rhodonite72				Mn (40)		Mn: +500,-800
Ni Metal	Ni (30)					Ni: \pm 500
Gahnite24	Zn (30)					Zn: \pm 500

Table A1.2: Spinel analytical conditions used on the University of Houston Cameca SX50 EMP. Number in parenthesis next to elements represent the measurement count time for that element. TAP: Thallium Acid Pthalate; PET: Pentaerythritol; LiF: Lithium Fluoride

Olivine Analytical Conditions						Accelerating Potential: 15 kV
Texas A&M University			Spot Size: 1 μ m		Beam Current: 20 nA	
Standard	SP1 (TAP)	SP2 (TAP)	SP3 (PET)	SP4 (LIF)	Backgrounds	
3olivine	Mg (40)	Si (40)		Fe (20)	Mg: \pm 1600; Si: +850,-800; Fe: \pm 500	
3chromite		Al (100)			Al: \pm 800	
5diopside			Ca (70)		Ca: \pm 600	
3ilmenite			Ti (70)		Ti: \pm 500	
7ni				Ni (60)	Ni: \pm 500	
5spessartine				Mn (60)	Mn: \pm 500	

Table A1.3: Olivine analytical conditions used on the Texas A&M University Cameca SX100 EMP. Number in parenthesis next to elements represent the measurement count time for that element. TAP: Thallium Acid Pthalate; PET: Pentaerythritol; LiF: Lithium Fluoride

Clinopyroxene Analytical Conditions						Accelerating Potential: 15 kV
Texas A&M University			Spot Size: 1 μ m		Beam Current: 20 nA	
Standard	SP1 (TAP)	SP2 (TAP)	SP3 (PET)	SP4 (LIF)	Backgrounds	
5albite	Na (20)				Na: \pm 700	
5diopside	Mg (60)	Si (45)	Ca (30)		Mg: \pm 1600; Si: \pm 850; Ca: \pm 600	
5orthoclase		Al (45)	K (30)		Al: \pm 800; K: \pm 500	
3ilmenite			Ti (30)		Ti: \pm 500	
3chromite				Cr (30)	Cr: \pm 500	
5spessartine				Mn (30)	Mn: \pm 500	
3olivine				Fe (30)	Fe: \pm 500	

Table A1.4: Clinopyroxene analytical conditions used on the Texas A&M University Cameca SX100 EMP. Number in parenthesis next to elements represent the measurement count time for that element. TAP: Thallium Acid Pthalate; PET: Pentaerythritol; LiF: Lithium Fluoride

Orthopyroxene Analytical Conditions					Accelerating Potential: 15 kV
Texas A&M University			Spot Size: 1 μ m		Beam Current: 20 nA
Standard	SP1 (TAP)	SP2 (TAP)	SP3 (PET)	SP4 (LIF)	Backgrounds
5albite	Na (20)				Na: \pm 700
3hypersth	Mg (60)	Si (45)			Mg: \pm 1600; Si: \pm 850
5diopside			Ca (30)		Ca: \pm 600
5orthoclase		Al (45)	K (30)		Al: \pm 800; K: \pm 500
3ilmenite			Ti (30)		Ti: \pm 500
3chromite				Cr (30)	Cr: \pm 500
5spessartine				Mn (30)	Mn: \pm 500
3olivine				Fe (30)	Fe: \pm 500

Table A1.5: Orthopyroxene analytical conditions used on the Texas A&M University Cameca SX100 EMP. Number in parenthesis next to elements represent the measurement count time for that element. TAP: Thallium Acid Pthalate; PET: Pentaerythritol; LiF: Lithium Fluoride

Spinel Analytical Conditions					Accelerating Potential: 15 kV
Texas A&M University			Spot Size: 1 μ m		Beam Current: 20 nA
Standard	SP1 (TAP)	SP2 (TAP)	SP3 (PET)	SP4 (LIF)	Backgrounds
3chromite	Mg (60)	Al (60)	Cr (30)	Fe (30)	Mg: \pm 1600; Al: \pm 800; Cr: \pm 500; Fe: \pm 500
5diopside		Si (60)	Ca (10)		Si: \pm 850; Ca: \pm 600
5spessartine			Mn (40)		Mn: \pm 500
3ilmenite			Ti (40)		Ti: \pm 500
V				V (30)	V: \pm 500
7ni				Ni (30)	Ni: \pm 500
3gahnite				Zn (30)	Zn: \pm 500

Table A1.6: Spinel analytical conditions used on the Texas A&M University Cameca SX100 EMP. Number in parenthesis next to elements represent the measurement count time for that element. TAP: Thallium Acid Pthalate; PET: Pentaerythritol; LiF: Lithium Fluoride

The Cameca software package applied a ZAF correction to the data after collection. Fe was speciated into FeO and Fe₂O₃ based on stoichiometry for each respective mineral following ZAF correction. The standard deviations of each oxide analysis of each sample (i.e. thin section) was used to calculate the reproducibility. The uncertainty of every oxide measurement over the measurement period was calculated by averaging the standard deviations for each individual sample. The individual reproducibility or uncertainty for each oxide can be found in major and minor element tables (Tables 2 - 4) in the Results section of this thesis. Mechanical drift, sample heterogeneity, as well as compositional differences between the samples and the standards can account for variances in accuracy.

The precision of measurements on during EMP analysis, is a function of x-ray counting statistics which in turn are a function of the total number of x-ray counts collected on both the calibration standard, and on the counts collected on the sample. The mechanical reproducibility of the spectrometers mostly limits measurement precision; however, low numbers of x-ray counts can be a factor in limiting counting statistics errors. As well, filament instability in addition to chemical heterogeneities both in samples and the standard can be major factors in the precision of EMP analysis. In order to determine the precision of both electron microprobes, Repeat analyses of secondary standards were performed (Table A1.7 – A1.5) in order to determine the precision of both EMPs used in this study.

Laser Ablation-Inductively Coupled Plasma Mass Spectrometry (LA-ICP-MS)

Time-resolution, in-situ analyses were performed on each clinopyroxene grain listed in table 5 of the Results section of this thesis. The analyses shown in table 5 are reported as averages of several spots (2-4) on a clinopyroxene grain within each sample. Each analytical session was begun with 3 spots on tholeiitic basalt glass standard (KL2-G), which was used as a reference standard, followed by analyses of dredge D31 clinopyroxenes, then finally ending with three spots on the KL2-G reference standard to correct and check for instrumental drift. Each spot analysis consists of three parts.

- (1) A ~10 second interval with the laser off is collected to measure the blank, or the He+Ar carrier gas).
- (2) The laser is turned on and the clinopyroxene is ablated. The ablated material is carried into the source by the carrier gas and measured for ~30-35 seconds.
- (3) The laser is turned off, and the elemental measurements are allowed to 'wash out' over an interval of 15-20 seconds.

Laser ablation of the samples used a CETAC laser ablation sample introduction system with a laser wavelength of 213 nanometers. The laser was set to a frequency of 5 hz which allowed for 150-175 bursts over a period of 30-35 seconds to hit the clinopyroxene.

An in-house data reduction program which identifies which part of the time-resolved elemental spectrum corresponds to actual clinopyroxene analysis and which part corresponds to background data was used to reduce the raw data for each analysis. The elemental intensities are corrected for the background by subtracting the average counts per second of the (Cps) background, or blank, measurement from the Cps of sample analyses.

Calcium (^{43}Ca) is used as an internal standard element (known from EMPA) to convert the background-corrected elemental intensities to concentrations by weight percent element (in ppm) using the following formula:

$$C_i^{Sa} = C_S^{Sa} \times \frac{I_i^{Sa}}{I_S^{Sa}} \times \frac{C_i^R}{C_S^R} \times \frac{I_S^R}{I_i^R}$$

where C_S^{Sa} is the concentration of the internal standard in the sample (calcium) determined by EMPA, I_i^{Sa}/I_S^{Sa} is the ratio of background-corrected intensity (Cps) of the element i to the internal standard element (calcium) in the sample. C_i^R/C_S^R is the ratio of the concentrations of the element i to the concentration of the internal standard in the reference standard, and I_S^R/I_i^R is the ratio of the background-corrected intensities of the internal standard element to the element i in the reference standard. Each individual spot is subjected to this conversion. The results are given in parts per million (ppm) and can be found in Table 7 within the main body of this thesis. Data rejection occurs automatically within the in-house program as well as by personal inspection of the programs output data.

Appendix 2: Petrographic Observations

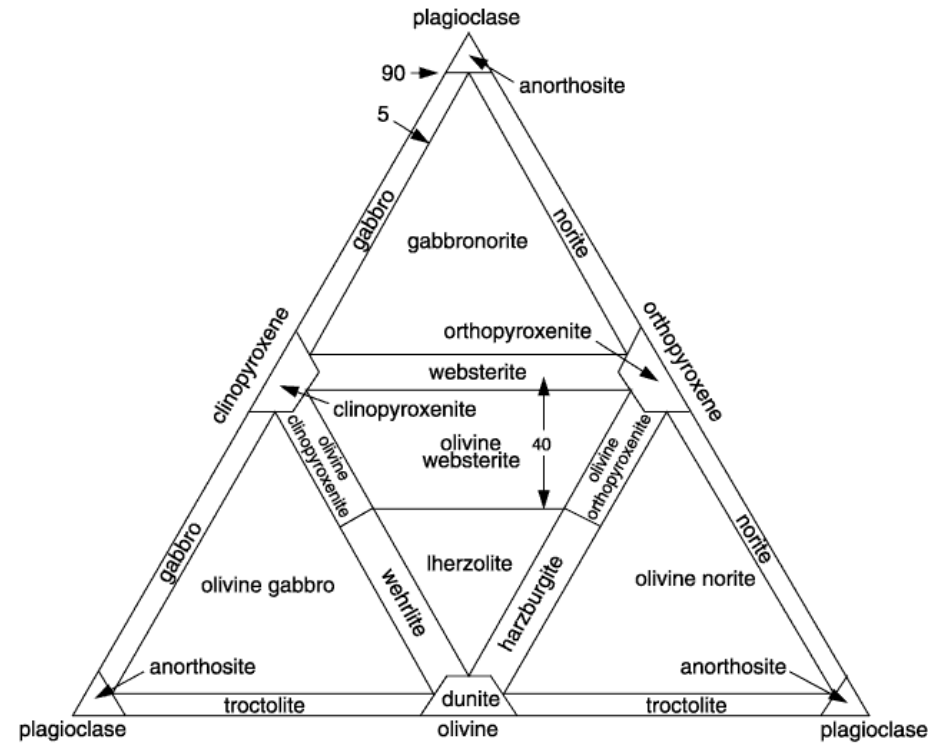


Figure A2.1: The combined ternary diagram for the classification of ultramafic and mafic rocks (Streckeisen, 1967). The following tables identify sample lithology on the basis of this IUGS classification.

Table A2.2: Summary of thin section descriptions (1 of 3)

Sample	Reason	Phases							Alt ¹	Def ²	%Ox ³	Description/Notes
		x- present, (x)-relict										
		OI	Opx	Cpx	Plag	Sp	Amp					
D31-001	too thin											
D31-002(2)	Peridotite (maybe dunite)		(x)		(x)	x				0.6		
D31-002(2)	Peridotite (maybe dunite)		(x)		(x)	x				0.5		
D31-003	too thin											
D31-004	Harzburgite	x	x	x		x		1.5	2	0.6	equigranular	
D31-007	Peridotite					x		4.5		0.6		
D31-009	Dunite		(x)			(x)		4.9		0.8	equigranular; spinel foliation; mostly former olivine	
D31-010	Harzburgite	x	x	x		x		4	4	0.7	bimodal- large opx (~5 to 10 mm) and smaller matrix of px and ol; spinel and opx phenocryst foliation	
D31-011(2)	Peridotite		(x)			x		5		0.4	equigranular; mostly former olivine with some opx	
D31-011(2)	Peridotite		(x)			x		5		0.3	equigranular; mostly former olivine with some opx	
D31-012	Pyroxenite		x			x		5	2	0.1		
D31-013	Dunite/Opx-Dunite		(x)			x		5	(3 to 4)	0.3	foliated (protomylonite); mostly former olivine (possible opx); spinels elongate parallel to foliation (deformation)	
D31-015	Peridotite		(x)			x		5		0.3		
D31-020	Harzburgite		(x)			x		5	4	0.3	Bimodal- large blocky Opx phenocrysts (~3 to 7 mm) and smaller olivine and opx; spinels elongated parallel to length of more blocky opx phenocrysts	
D31-021	Dunite	x				x		4.5	4	0.3	former olivine very large; possible foliation in spinels (length oriented although more rounded); spinels contain inclusions of fresh silicates	
D31-021(2)	Dunite					x				1.5	former olivine very large; possible foliation in spinels (length oriented although more rounded)	
D31-022	Dunite					(x)		5		0.4	protomylonite; veins filled with talc (growth structures parallel to fracture wall); spinels exhibit possible length foliation; evidence for very little former px	
D31-024	Dunite/Opx-Dunite		x			x		5	4	0.8	possible spinel foliation; relict opx is diffuse and appears to be "feathered" in between former olivine; very little former opx	
D31-025	Dunite					x		5		0.8	no apparent foliation; all olivine with a few large, rounded spinels	
D31-026	Dunite					x		5	4	0.8	protomylonite; spinels with no apparent foliation...less deformed, more rounded spinels	
D31-026a	Dunite					x		5		0.2	protomylonite; spinels with no apparent foliation...less deformed, more rounded spinels	

1 Alteration Scale: 0- Totally fresh; 1- Some secondary phases; 2- Abundant secondary phases; 3- Complete eradication of a phase; 4- Some primary phases left; 5- No primary phases left.

2 Deformation Scale: 0- Undeformed; 1- Some deformation textures; 2- Abundant deformation textures; 3- Onset of recrystallization; 4- Pervasive recrystallization, foliation; 5- Grain size reduction, strong foliation.

3 Volume percent of oxides estimated with ImageJ software. Procedure for modal estimation provided by Roeder et al. (2006).

Table A2.2: Summary of thin section descriptions (2 of 3)

Table A.12. Summary of thin section descriptions (2 of 4)											
Sample	Reason	Phases						Alt ¹	Def ²	%Ox ³	Description/Notes
		<i>x- present, (x)-relict</i>									
		Ol	Opx	Cpx	Plag	Sp	Amp				
D31-031	Harzburgite	x	x	x		x		3	3	3.2	equigranular; some opx but mostly olivine and spinel; spinel ranges from blocky to rounded
D31-035	Harzburgite		(x)		x	x		5	4	0.4	protomylonite and fracturing of larger grains; spinels foliated parallel to rock deformation; mostly altered olivine with some pyroxene
D31-101	Wehrlite	x		x	x	x		3	1	0.2	cpx and minor plag, but mostly olivine; px grains embayed by altered plagioclase in the interstices; cpx in better shape than olivine; estimation of melt impregnation- ~1 to 5 %
D31-102	Pl-wehrlite	x		x	x	(x)		4		<0.1	relict/bastite larger cpx grains amongst serpentinized olivine/dunite; small diffuse areas and patches of altered plagioclase; transition over thin section from areas of larger cpx grains to areas of larger plag patches
D31-103	Pl-wehrlite	x		x	x	x				0.6	poikilitic texture of olivine (dunite) crystals within cpx and plagioclase; Portions of section contain large cpx oikocrysts and others contain less poikilitic textures with plagioclase in the interstices; regions with plagioclase contain less rounded olivines with a more equigranular texture whereas the cpx regions contain granular olivine with resorption/cumulate textures. There is a gradation between these regions. possibly fresh plag, but for sure fresh cpx.
D31-104	Wehrlite/dunite	x		x	x	x		4		0.5	relict/bastite larger cpx grains amongst serpentinized olivine/dunite; small diffuse areas and patches of altered plagioclase; transition over thin section from areas of larger cpx grains to areas of larger plag patches
D31-105	Pl-wehrlite	x		x	x	x		5		1.2	large patches of altered plagioclase between olivines with resorption textures, possible spinel foliation; spinels contain relict silicate inclusions; some patches of plag have blocky boundaries
D31-106	Pl-wehrlite	x		x		x		4		<0.1	poikilitic texture of a few very large cpx oikocrysts enclosing olivine; patches of granular olivine and patches of larger more blocky olivine; cpx is better preserved around larger blocky olivine, possibly some diffuse patches of plagioclase but not as extreme as cpx; infiltration textures of cpx into dunite
D31-107	Ol-gabbro	x	(x)	x	x	x		4		0.9	melt infiltration into an equigranular cpx-bearing harzburgite; portions of section are have small amount of opx (maybe noritic); resorption textures of olivine and opx into plagioclase patches; overall sample is cpx + plag with some minor ol and opx
D31-108	Gabbro/cataclasite			x	x			4	2	<0.1	large cataclasite on right portion of section (dominantly cpx phenocrysts); obvious deformation in sample; large altered cpx grains with evidence of shear amongst a mix of smaller plag and cpx grains and a sheared matrix; heavily fractured

1 Alteration Scale: 0- Totally fresh; 1- Some secondary phases; 2- Abundant secondary phases; 3- Complete eradication of a phase; 4- Some primary phases left; 5- No primary phases left.

2 Deformation Scale: 0- Undeformed; 1- Some deformation textures; 2- Abundant deformation textures; 3- Onset of recrystallization; 4- Pervasive recrystallization, foliation; 5- Grain size reduction, strong foliation.

3 Volume percent of oxides estimated with ImageJ software. Procedure for modal estimation provided by Roeder et al. (2006).

Table A2.2: Summary of thin section descriptions (3 of 3)

Sample	Reason	Phases <i>x</i> -present, (<i>x</i>)-relict						Alt ¹	Def ²	%Ox ³	Description/Notes
		OI	Opx	Cpx	Plag	Sp	Amp				
D31-201	Pyroxenite	(x)	x	x	(x)	x		4	3	0.1	equigranular pyroxenite (bastite with minor relics); some relic opx and cpx; a few large spinels; evidence of shear fractures filled with talc; Grain boundaries range from flat to deeply embayed- evidence of grain boundary diffusion (med Temp deformation)
D31-301	Pl-dunite/Clinopyroxenite	x		x	x	(x)		3.75	1	0.1	a very large cpx grain intruded by blocky to amorphous plagioclase patches against a plagioclase impregnated dunite
D31-302	OI-gabbro	x	(x)		(x)	x		2	1	0.8	poikilitic texture of large cpx oikocrysts surrounding granular olivine; some patches of blocky olivine with minor plagioclase in between some of the oikocrysts; minor spinel; grain boundaries between opx oikocrysts are irregular ; Olivine within oikocrysts are better preserved
D31-303	Gabbro	x		x	x	x		2	2	0.8	a few small Fe-Ti oxides; poikilitic texture of large cpx oikocrysts surrounding plagioclase crystals; oikocryst boundaries are irregular and tend to have large concentrations of plagioclase crystals; possibly two generations of plag- larger blocky crystals in interstices and in aggregates and smaller more lathe-like crystals: Ophitic texture
D42-101	Gabbro		(x)	(x)	x	x	x	5	1	1.1	
D42-101	Gabbro		(x)	(x)	x	x	x	5	1	1.9	
D42-101	Dunite	x	(x)			x		4	4	1.3	
D42-102	Gabbro		x	x		x	x			1.2	
D42-103	Oxide Gabbro	x	x	x	x	x	x	4	2	5	
D42-104	(Ox) Gabbro	x	x	x	x	x	x	4	2	1.2	
D42-105	(Ox) Gabbro	x	x	x	x	x	x	4	2	0.9	
D42-106	Oxide Gabbro	x	x	x	x	x	x	4	2	4.5	
D42-107	Gabbro	x	x	x	x	x	x	4	2	0.7	
D42-108	Gabbro		x	x	x	x	x	4	2	0.5	
D42-109	Gabbro		x	x	x	x	x	4.5	2	0.4	
D42-110	Gabbro		x	x	x	x	x	4.5	2	1	
D42-111	Oxide Gabbro		x	x	x	x	x	4	2	3.5	
D42-112	Gabbro	x	x	x	x	x	x	4	3	0.7	
D42-112	(Ox) Gabbro	x	x	x	x	x	x	4	2	0.5	

1 Alteration Scale: 0- Totally fresh; 1- Some secondary phases; 2- Abundant secondary phases; 3- Complete eradication of a phase; 4- Some primary phases left; 5- No primary phases left.

2 Deformation Scale: 0- Undeformed; 1- Some deformation textures; 2- Abundant deformation textures; 3- Onset of recrystallization; 4- Pervasive recrystallization, foliation; 5- Grain size reduction, strong foliation.

3 Volume percent of oxides estimated with ImageJ software. Procedure for modal estimation provided by Roeder et al. (2006).

